

# Open Research Online

---

The Open University's repository of research publications and other research outputs

## Water in evolved lunar rocks: Evidence for multiple reservoirs

### Journal Item

How to cite:

Robinson, Katharine L.; Barnes, Jessica J.; Nagashima, Kazuhide; Thomen, Aurélien; Franchi, Ian A.; Huss, Gary R.; Anand, Mahesh and Taylor, G.Jeffrey (2016). Water in evolved lunar rocks: Evidence for multiple reservoirs. *Geochimica et Cosmochimica Acta*, 188 pp. 244–260.

For guidance on citations see [FAQs](#).

© 2016 Elsevier

Version: Not Set

Link(s) to article on publisher's website:  
<http://dx.doi.org/doi:10.1016/j.gca.2016.05.030>

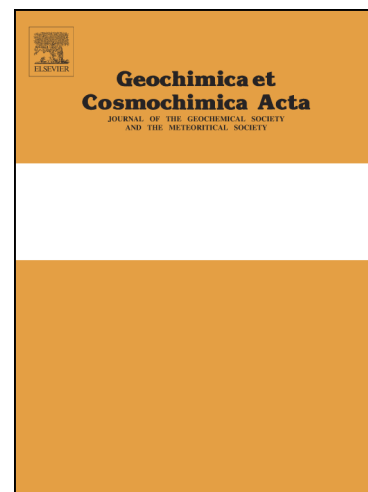
---

Copyright and Moral Rights for the articles on this site are retained by the individual authors and/or other copyright owners. For more information on Open Research Online's data [policy](#) on reuse of materials please consult the policies page.

---

[oro.open.ac.uk](http://oro.open.ac.uk)

## Accepted Manuscript



Water in evolved lunar rocks: Evidence for multiple reservoirs

Katharine L. Robinson, Jessica J. Barnes, Kazuhide Nagashima, Aurélien Thomen, Ian A. Franchi, Gary R. Huss, Mahesh Anand, G. Jeffrey Taylor

PII: S0016-7037(16)30273-3  
DOI: <http://dx.doi.org/10.1016/j.gca.2016.05.030>  
Reference: GCA 9779

To appear in: *Geochimica et Cosmochimica Acta*

Received Date: 26 June 2015  
Accepted Date: 16 May 2016

Please cite this article as: Robinson, K.L., Barnes, J.J., Nagashima, K., Thomen, A., Franchi, I.A., Huss, G.R., Anand, M., Jeffrey Taylor, G., Water in evolved lunar rocks: Evidence for multiple reservoirs, *Geochimica et Cosmochimica Acta* (2016), doi: <http://dx.doi.org/10.1016/j.gca.2016.05.030>

This is a PDF file of an unedited manuscript that has been accepted for publication. As a service to our customers we are providing this early version of the manuscript. The manuscript will undergo copyediting, typesetting, and review of the resulting proof before it is published in its final form. Please note that during the production process errors may be discovered which could affect the content, and all legal disclaimers that apply to the journal pertain.

## Water in evolved lunar rocks: Evidence for multiple reservoirs

Katharine L. Robinson<sup>\*,a,b,c</sup>, Jessica J. Barnes<sup>d,e</sup>, Kazuhide Nagashima<sup>a</sup>, Aurélien Thomen<sup>a</sup>, Ian A. Franchi<sup>e</sup>, Gary R. Huss<sup>a,b,c</sup>, Mahesh Anand<sup>d,e</sup>, G. Jeffrey Taylor<sup>a,b,c</sup>

<sup>a</sup> Hawaii Institute of Geophysics and Planetology, 1680 East-West Rd. POST 602, Honolulu, HI 96822, USA

<sup>b</sup> University of Hawaii NASA Astrobiology Institute, Institute for Astronomy, University of Hawai'i, 2680 Woodlawn Drive, Honolulu, Hawaii 96822-1839, USA.

<sup>c</sup> Geology and Geophysics, University of Hawaii at Manoa, 1680 East-West Rd. POST 602, Honolulu, HI 96822, USA

<sup>d</sup> Planetary and Space Sciences, The Open University, Walton Hall, Milton Keynes, MK7 6AA, UK,

<sup>e</sup> Department of Earth Sciences, The Natural History Museum, Cromwell Road, London, SW7 5BD, UK.

\*Corresponding Author: Katharine Robinson

\*Now at Planetary and Space Sciences, The Open University.

email: krobenson@higp.hawaii.edu

phone: (812) 251-7409

Manuscript submitted to *Geochimica et Cosmochimica Acta* June 2015

Revised and resubmitted, March 2016

Revised and resubmitted, May 2016

Main text, references, table, and figure captions

**Water in evolved lunar rocks: Evidence for Multiple Reservoirs****1 Abstract**

2 We have measured the abundance and isotopic composition of water in apatites from  
3 several lunar rocks representing Potassium (K), Rare Earth Elements (REE), and Phosphorus (P) -  
4 KREEP - rich lithologies, including felsites, quartz monzodiorites (QMDs), a troctolite, and alkali  
5 anorthosite. The H-isotope data from apatite provide evidence for multiple reservoirs in the  
6 lunar interior. Apatite measurements from some KREEP-rich intrusive rocks display moderately  
7 elevated  $\delta D$  signatures, while other samples show  $\delta D$  signatures similar to the range known for  
8 the terrestrial upper mantle. Apatite grains in Apollo 15 quartz monzodiorites have the lowest  
9  $\delta D$  values measured from the Moon so far (as low as - 749 ‰), and could potentially represent  
10 a D-depleted reservoir in the lunar interior that had not been identified until now. Apatite in all  
11 of these intrusive rocks contains < 267 ppm H<sub>2</sub>O, which is relatively low compared to apatites  
12 from the majority of studied mare basalts (200 to > 6500 ppm H<sub>2</sub>O). Complexities in  
13 partitioning of volatiles into apatite make this comparison uncertain, but measurements of  
14 residual glass in KREEP basalt fragments in breccia 15358 independently show that the KREEP  
15 basaltic magmas were low in water. The source of 15358 contained ~ 10 ppm H<sub>2</sub>O, about an  
16 order of magnitude lower than the source of the Apollo 17 pyroclastic glass beads, suggesting  
17 potential variations in the distribution of water in the lunar interior.

**18 1. Introduction.**

19 The detection of water in lunar volcanic glasses, apatites, and melt inclusions has  
20 implications for planetary accretion, the source(s) of water in the Earth-Moon system, and the  
21 role of water in lunar evolution (Saal et al., 2008; McCubbin et al., 2010; Boyce et al., 2010;  
22 Greenwood et al., 2011; Hauri et al., 2011; Tartèse et al., 2013, 2014; Barnes et al., 2013,  
23 2014a). (In this paper we use “water” as a shorthand way of referring to all hydrogen species,  
24 H<sub>2</sub>O, OH, and H<sub>2</sub>. More than one may be present, depending on oxygen fugacity and pressure  
25 (e.g., Hirschmann et al., 2012.) Recent work has shown that apatites in mare basalts contain  
26 appreciable amounts of water, and are generally enriched in deuterium (<sup>2</sup>H, or D) with respect

27 to Earth, possibly due to the addition of D-rich material early in the Moon's history (Greenwood  
28 et al., 2011) or to the loss of H preferentially over D during magma degassing (e.g. Saal et al.  
29 2008; Tartèse and Anand, 2013; Tartèse et al., 2013, Saal et al., 2013). The final fraction of the  
30 global lunar magma ocean (LMO) model is considered to be urKREEP, so named for its  
31 enrichment in incompatible elements compared to other lunar materials (e.g., Warren and  
32 Wasson, 1979). Because water behaves as an incompatible element in major silicate phases  
33 that formed during the LMO crystallization (Koga et al., 2003; Aubaud et al., 2004; Grant et al.  
34 2007), KREEP-rich rocks are expected to be enriched in water relative to other lunar rocks.  
35 Many KREEP-rich lithologies consist of evolved rocks that formed as intrusions, which means  
36 that they would have avoided or experienced minimal water loss (unlike the mare basalts), and  
37 potential hydrogen isotope fractionation due to magmatic degassing.

38 The mineral apatite  $[\text{Ca}_5(\text{PO}_4)_3(\text{F},\text{Cl},\text{OH})]$  incorporates OH into its crystal structure, making  
39 it a potential recorder of the concentration of OH in magma at the time of apatite  
40 crystallization. The OH in apatite is resistant to exchanging O or H with adsorbed terrestrial  
41 water on thin section surfaces (Greenwood et al., 2011) hence it is useful for H isotopic  
42 measurements by secondary ion mass spectrometry (SIMS). The D/H ratio, expressed as  $\delta\text{D}$  (‰)  
43  $= ([\text{D}/\text{H}]_{\text{sample}}/[\text{D}/\text{H}]_{\text{standard}} - 1) \times 1000$ , relative to Vienna Standard Mean Ocean Water (V-  
44 SMOW), is important for identifying the source of the Moon's water and the extent of water  
45 loss during magmatic processing (e.g., Greenwood et al., 2011; Elkins-Tanton and Grove, 2011;  
46 Tartèse et al., 2013). Previous studies have demonstrated that the water content of lunar  
47 apatite varies among different rock types. Apatites in Apollo mare basalts record the highest  
48  $\text{H}_2\text{O}$  contents (up to ~7500 ppm) and  $\delta\text{D}$  (+390 to +1100‰) (McCubbin et al., 2010;  
49 Greenwood et al., 2011,; Barnes et al., 2013; Tartèse et al., 2013), while apatites in more  
50 evolved, KREEP-related rocks generally have lower  $\text{H}_2\text{O}$  contents (< 3000 ppm) and  $\delta\text{D}$  values (-  
51 384 to +791‰, Greenwood et al., 2011; Barnes et al., 2014a; Tartèse et al., 2014; Robinson et  
52 al., 2013, Robinson and Taylor, 2014).

53 Though it was initially thought that apatite water contents could be used to infer initial  
54 magmatic water abundances (McCubbin et al., 2010, Boyce et al., 2010, Tartèse et al, 2013,

55 2014, Barnes et al. 2014a), Boyce et al. (2014) demonstrated that the F-Cl-OH partitioning into  
56 apatite is not well-described by a simple apatite-melt partition coefficient. Apatite water  
57 content thus cannot be used to quantitatively determine the amount of water in the co-existing  
58 melt, unless the F or Cl content are also known for both melt and apatite, and that it can be  
59 confirmed that apatite crystallized in equilibrium with the melt. However, the measured D/H  
60 ratios are still useful for gaining insights into processes that might have affected the parental  
61 magmas.

62 Rocks formed in an intrusive environment could have experienced minimal D-H  
63 fractionation and water loss prior to apatite crystallization because they form at pressures  
64 where water is far more soluble in silicate melt than at low pressures near or on the surface  
65 (e.g., Dixon et al., 1995). Water solubility in magmas decreases with decreasing pressure, so  
66 when a hydrous magma approaches a planetary surface, the melt degasses and water is lost  
67 assuming water is present as OH and H<sub>2</sub>O. Diffusion modelling of water loss from volcanic lunar  
68 pyroclastic glasses indicates that they lost up to 98% of their initial water content upon  
69 eruption (Saal et al., 2008). Mare basaltic magmas would also have degassed during eruption  
70 onto the lunar surface, but probably less than the 98% loss experienced by pyroclastic glasses.  
71 Based on water contents of melt inclusions in olivine from subaerial and submarine Hawaiian  
72 lavas (which have little water loss due to the pressure at which they erupted; Hauri 2002), we  
73 estimate that lava flows lose up to 90% of their pre-eruptive H<sub>2</sub>O. Low-Ti mare magmas could  
74 have lost 85 to 99% of their pre-eruptive water contents (Tartèse et al., 2013), but such  
75 estimates assume an initial D/H ratio. The degassing of hydrogen from a magma or lava also  
76 fractionates lighter H from heavier D, especially if H<sub>2</sub> is lost rather than H<sub>2</sub>O (e.g. Richet et al.,  
77 1977; Tartèse and Anand 2013; Tartèse et al., 2013). Degassing experiments with apatite  
78 suggest that volatile loss occurs rapidly in extrusive magmas, and that apatite, which forms late,  
79 will not preserve pre-eruption volatile contents and will instead reflect the post-degassing  
80 volatile composition of the magma (Ustunisik et al., 2015). The erupted mare basalts have the  
81 highest  $\delta D$  values (up to  $\sim +1100\text{‰}$ ) found in lunar rocks so far (Greenwood et al., 2011; Barnes  
82 et al., 2013; Tartèse et al., 2013).

83 Apatite in intrusive rocks may represent a more pristine sampling of the lunar interior  
84 water than the water bound in apatites in the mare basalts, due to their formation at depth at  
85 higher pressures (Robinson et al., 2013; Robinson and Taylor, 2014; Barnes et al., 2014a).  
86 Reaction relations in symplectitic intergrowths in troctolite 76535 indicate a depth of origin of  
87 ~40 km (Gooley et al., 1974; McCallum et al., 2006), corresponding to a pressure of over 1.5 kb.  
88 On the other hand, gabbro-norite sample 76255 may have formed as shallow as a few  
89 kilometers (McCallum et al., 2006), and quartz-monzodiorite 14161,7373 as shallow as 1 km  
90 (Jolliff et al., 1999), at a pressure of 50 b. The liquidus temperatures and presence of quartz in  
91 highly fractionated lunar felsites (Hess et al., 1975; Hess et al. 1978; Hess et al. 1989; Robinson  
92 and Taylor, 2011; Robinson et al., 2015) indicate crystallization at a pressure of at least ~1 kb  
93 (Tuttle and Bowen, 1958), corresponding to a depth of over 20 km, assuming a crustal density  
94 of 2550 kg/m<sup>3</sup> (Wieczorek et al., 2013). Up to 3 wt. % H<sub>2</sub>O is soluble in rhyolitic melts at ~1kb,  
95 and even 0.5 wt.% would have been soluble at the 50 b pressure experienced by the parental  
96 melt for QMD 14161, 7373 (VolatileCalc, Newman and Lowenstern 2002; Jolliff et al. 1999).  
97 Common mineral phases associated with hydrous melts such as amphibole and micas have  
98 never been reported in lunar rocks, and no lunar magma has been shown to have contained  
99 weight percent levels of water (e.g. Robinson and Taylor, 2014 and references therein). While  
100 the concentration of water in the melt would have increased during crystallization, it would  
101 have had to reach weight percent levels to degas *before* apatite crystallization began and  
102 removed F, Cl, and OH from the melt (Boyce et al., 2014). Assuming that water is completely  
103 incompatible in the crystallizing silicates and that a magma had an initial H<sub>2</sub>O content of 0.1  
104 wt% (similar to A17 melt inclusions, Saal et al., 2013), the H<sub>2</sub>O concentration would have only  
105 increased to 1 wt.% after 90% crystallization. Apatite forms after 90% crystallization in basaltic  
106 systems, and earlier in KREEP-rich melts (Harrison and Watson, 1984; Tartèse and Anand, 2013;  
107 Tartèse et al. 2014). Unless they were exceptionally water-rich, water would have remained  
108 soluble in the parental melts for all the KREEP-rich intrusive rocks discussed here.

109 While H loss by degassing may not occur in the KREEP-rich intrusive rocks, their H isotopes  
110 could be affected by diffusion. Studies of melt inclusions in basalts show that lighter H can  
111 escape from melt inclusions by diffusion, therefore enriching heavier D in the melt inclusion

112 over time (Gaetani et al., 2012, Bucholz et al., 2013). It is unclear if a similar process affected  
113 the H isotopes in apatite from the KREEP-rich intrusive rocks, or if H from country rock  
114 surrounding the magma bodies could have been incorporated. However, in order for H to be  
115 lost (or gained), it would have to diffuse through either a liquid or solid medium. This would  
116 have a less extreme fractionation effect than degassing into vacuum or a low-pressure  
117 environment (Bucholz et al., 2013). A magmatic system is more complex than a melt inclusion,  
118 and some water loss and H isotope fractionation might occur, but apatite in a rock formed  
119 intrusively is generally more likely to have retained the isotopic composition of lunar interior  
120 water than rapidly degassed samples such as apatite in mare basalts or glass in pyroclastics.

121 If water was present in the lunar magma ocean, it should be highly concentrated in KREEP-  
122 rich materials, assuming no significant loss occurred during magma ocean crystallization and  
123 subsequent cumulate overturn (Tartèse et al., 2014). Anything KREEP-rich or derived from  
124 KREEP basaltic magmas should also be enriched in water. However, it is not a simple path from  
125 late-stage magma ocean products to KREEP-rich or KREEP-related magmas, which formed  
126 either by the assimilation of the urKREEP component by rising Mg-rich diapirs at the base of the  
127 lunar crust, or by the partial melting of hybrid mantle sources, formed by sinking urKREEP (and  
128 other dense components) mixing with Mg-rich olivine-orthopyroxene cumulates (Shearer and  
129 Floss, 1999; Shearer and Papike, 2005; Elardo et al, 2011). Regardless of the formation  
130 mechanism, these magmas gave rise to what we now know as the KREEP basalts, and the  
131 norites and troctolites of the magnesian (Mg) suite (recently reviewed by Shearer et al., 2015).  
132 Fractional crystallization of magmas resembling KREEP basalts is thought to have produced  
133 geochemically evolved rocks such as quartz monzodiorites (Ryder, 1976; Ryder and Martinez,  
134 1991, Jolliff 1991). Alternatively, silicate liquid immiscibility (SLI) is proposed to have played a  
135 role in the formation of the lunar felsites (e.g., Hess et al., 1975, Warner et al., 1978 Snyder et  
136 al., 1995; Ryder and Martinez, 1991, Shearer et al., 2015). Most importantly, any petrologic  
137 processing took place inside the Moon at pressures high enough to inhibit water loss from  
138 magmas or mantle rocks.

139



140 **2. Samples.**

141 The felsites and quartz monzodiorites (QMDs) are both intrusive late-stage fractionates of  
142 KREEP-basaltic magmas (Ryder et al., 1975; Ryder and Martinez, 1991). The felsite suite  
143 consists of evolved Si-rich (~ 70 wt % SiO<sub>2</sub>) rocks with graphic intergrowths of quartz and K-  
144 feldspar (Ryder et al., 1975; Warner et al., 1978; Taylor et al., 1980; Warren et al., 1983, 1987;  
145 Jolliff 1991; Robinson and Taylor, 2011). Silica-rich compositions can be generated by partial  
146 melting, but extensive fractional crystallization also produces silica-rich melt through the  
147 process of silicate liquid immiscibility (SLI) (e.g. Rutherford et al., 1974). After 90-98%  
148 crystallization of a basaltic magma, the remaining liquid will spontaneously separate into Si-rich  
149 and Fe-rich liquids (FeO 12-14 wt. %; Roedder and Weiblen 1971, Hess et al. 1975). The Si-rich  
150 end member is called a felsite, while the Fe-rich end member is called a ferrobasalt (Rutherford  
151 et al., 1974). Based on felsite texture and the presence of quartz, rather than another silica  
152 polymorph, the felsites and their corresponding Fe-rich phases formed in small intrusive bodies  
153 through silicate liquid immiscibility of an evolving magma of KREEP-basalt composition (e.g.  
154 Warner et al., 1978; Taylor et al., 1980; Warren et al., 1983; Robinson and Taylor 2011).

155 Felsite sample 14321,1047 is well-known, consisting of clasts of graphically-intergrown  
156 quartz and K-feldspar, and resides in clast-rich impact breccia 14321 (Warren et al., 1983; Fig.  
157 1a). Apatite was found enclosed by quartz in Si-rich 14321,1047, suggesting that it was a  
158 liquidus phase. Sample 77538,16 is unique in that it preserves both silicate liquid immiscibility  
159 end-members in co-existing felsite and ferrobasalt areas (Warner et al. 1978)(Fig. 1b). Apatite  
160 was found in both the Si-rich and Fe-rich end members; it is enclosed in clinopyroxene in the  
161 Fe-rich regions of 77538 and in K-feldspar in the Si-rich regions of 77538.

162 The quartz monzodiorites (QMDs) are also evolved rocks. They exhibit a cumulate texture  
163 and are probably fractional crystallization products of KREEP basaltic magmas (Ryder and  
164 Martinez, 1991; Jolliff 1991), though not quite as extreme fractionates as the felsites. Many  
165 contain exsolved pyroxenes, indicating they formed in a slow-cooling, intrusive environment.  
166 Both 14161,7069 (Fig. 1d) and -,7373 were classified as QMDs (Jolliff 1991). Section  
167 14161,7373 is particularly notable for its inverted, exsolved pyroxenes and high phosphate

168 content, mostly in the form of whitlockite (Jolliff 1991); strictly speaking, this anhydrous  
169 phosphate is more properly called merrillite (Hughes et al., 2006; Jolliff et al., 2006; Hughes et  
170 al., 2008; McCubbin et al., 2014). Based on An contents of plagioclase some QMDs are  
171 probably more accurately described as monzogabbros, but we use monzodiorites here to  
172 maintain consistency with the majority of previously published literature on these samples.

173 We studied three QMD clasts from soil sample 15400, (15404,51, 15404,55 and 15403,71)  
174 which was likely derived from the top of a large boulder (sampled as 15405) at Station 6A on  
175 the Apollo 15 mission. Sample 15403,71 is a single fragment from the 2-4 mm fraction of  
176 15400. It consists of roughly 50% impact melt and 50% shocked QMD. The QMD contains large  
177 phosphates, including a single > 500  $\mu\text{m}$  apatite grain (Marvin et al., 1991). Sample 15404,51  
178 and ,55 come from the 4-10 mm size fraction. Apatite in QMD 15404,51 was studied previously  
179 by McCubbin et al. (2010). Sample 15404,55 (Fig. 1c) is also a QMD, from the same chip and  
180 lithology as 15404,51. In each of the three thin-sections studied, pyroxene shows fine  
181 exsolution lamellae, indicating an intrusive origin. Moreover, the samples' enrichment in rare  
182 earth elements (Lindstrom et al., 1992), relative to Apollo 15 KREEP basalts, show they probably  
183 formed via fractional crystallization of an Apollo 15 KREEP-like magma, as shown by previous  
184 studies (e.g., Ryder and Martinez, 1991; Taylor et al., 2012).

185 Alkali anorthosite clasts were studied in breccia 14305,656 (Fig.1f). The alkali anorthosites  
186 are also products of fractional crystallization of a KREEP-rich basaltic magma, thought to have  
187 formed as flotation cumulates in intrusive magma bodies (Shervais and McGee, 1999).  
188 Merrillite was reported in other alkali anorthosite sections of 14305 (Shervais and McGee,  
189 1999), and our thin-section seems to be particularly rich in merrillite. Apatite is intergrown with  
190 merrillite in sample 14305,656.

191 Troctolite 76535 is coarse-grained and shows signs of slow subsolidus annealing, leading to  
192 the interpretation that it could have formed at depths of tens of kilometers in the crust,  
193 significantly inhibiting water loss (Gooley et al., 1974; Dymek et al., 1975; Schwartz and  
194 McCallum, 1999). There are also reports that this rock may have been altered by post-  
195 crystallization metasomatism, which likely would have altered the magmatic volatile contents

196 of apatite in this rock (Elardo et al., 2012; Barnes et al., 2014a). We measured apatites in two  
197 thin-sections, 76535,52 and -,56 (Fig 1e). The troctolite is not directly derived from KREEP  
198 basaltic magma like the felsites or QMDs, but it does have a high-KREEP content as revealed by  
199 trace element analyses of mineral grains (Shearer and Floss, 1999).

200 We also examined two KREEP basalt fragments in impact melt breccia 15358,6. These  
201 KREEP basalts have intersertal to intergranular textures and abundant yellow glass that is  
202 interpreted to be the last 11-18 % of a KREEP basaltic melt, which quenched instead of  
203 crystallizing (Ryder 1988; Taylor et al. 2012). No evidence for the clasts being impact melt  
204 breccias, such as unmelted mineral fragments, is present (Taylor et al., 2012). Apatite large  
205 enough for SIMS analysis was not identified in either fragment; instead the D/H ratio and H  
206 concentration of the glass was measured. These unique clasts likely represent late-stage break  
207 outs from KREEP basalt lava flows (Taylor et al., 2012).

### 208 **3. Methods**

209 *3.1. Secondary Ion Mass Spectrometry (SIMS).* Two instruments, the Cameca ims-1280 and  
210 the NanoSIMS 50L, have both been successfully used to measure H isotopes in extraterrestrial  
211 apatite (e.g. Hallis et al., 2012; Robinson et al., 2012; Barnes et al., 2013; Tartèse et al., 2013;  
212 2014). The ims-1280 has higher analytical precision, but a large analysis size. The 50L  
213 NanoSIMS has a smaller analysis size, allowing the measurement of apatites that are too small  
214 or cracked to be analyzed with the ims-1280. This paper reports data from both instruments,  
215 and the respective protocols are described below.

216 *3.1.1. University of Hawaii (UH).* The protocol for measuring H isotopes in apatite at UH  
217 was developed for use with both Martian and lunar materials. A detailed description of this  
218 protocol can be found in Hallis et al. (2012). Lunar apatites were analyzed *in-situ* with the ims  
219 1280 secondary-ion mass spectrometer during four separate analytical sessions (May and  
220 November 2011, August 2012, and July 2014). We used a 2 nA Cs<sup>+</sup> primary beam (4 nA in  
221 August 2012 and July 2014). The secondary-ion mass spectrometer was operated at 10 keV  
222 (giving a 20 keV impact energy) with a 50 eV energy window. The mass resolving power was

223 ~1900 (defined as peak width at 10% of peak height), sufficient to separate any interfering  
224 molecular ions. A normal-incidence electron flood gun was used for charge compensation of  
225 the analyzed area.

226 Using a rastered beam, a  $25 \times 25 \mu\text{m}^2$  area was sputtered for 300 s to remove the carbon  
227 coat and any surface contaminants before the actual measurement took place. During the pre-  
228 sputtering, we monitored the H ion image to identify and then avoid any possible terrestrial  
229 contamination. In the H ion image, H-rich material such as epoxy or small cracks appears very  
230 bright. The beam was repositioned (when possible), in order to avoid H-rich areas. The  
231 measurement was aborted if no “clean” area could be identified.  $^1\text{H}^-$ ,  $^2\text{D}^-$ , and  $^{18}\text{O}^-$  were then  
232 measured sequentially on an electron multiplier in monocollection mode from a reduced  
233 rastered area of  $15 \times 15 \mu\text{m}^2$ . For glass measurements, ions of  $^{30}\text{Si}^-$ , instead of  $^{18}\text{O}^-$  were  
234 collected. An electronic gate was used to exclude counts from all but the inner  $\sim 8 \times 8 \mu\text{m}^2$  of  
235 this area to avoid the edges of the sputtered pit and H creep across the sample surface. If  
236 contamination appeared (as a very bright signal on the H image and/or a sudden large spike in  
237 the H count rate) during the course of a measurement, the affected cycles were eliminated  
238 during data reduction.

239 Each measurement consisted of 40 cycles.  $^1\text{H}$  was counted for 3 s, D for 40 s, and  $^{18}\text{O}$  (or  
240  $^{30}\text{Si}$  for glasses) for 2 s in each cycle. The primary beam was blanked for the first 10 and final 5  
241 cycles in order to measure background H and D signals (mainly contributed by the electron  
242 gun). The background counts were subtracted from the measured isotope signal, which was  
243 collected between cycles 11 and 35 while the beam was positioned on the sample. We made  
244 appropriate corrections in data analysis to account for the electronic gate and deadtime of the  
245 electron multiplier (c.f. Hallis et al., 2012). Hydrogen isotopes of KREEP basalt glasses were  
246 measured on the same instrument in March 2012 using the same analytical conditions.

247 The SIMS measurements were calibrated prior to lunar apatite measurements using 3  
248 natural terrestrial apatite standards (Ap003 Durango, Ap018 Russia, and Ap005 Crystal Lode),  
249 mounted in epoxy, that were characterized previously by McCubbin et al. (2012). Ap018 and  
250 Ap005 were also used for instrumental mass fractionation corrections of measured D/H ratios.

251 The H<sub>2</sub>O content of lunar apatite was determined from their measured <sup>1</sup>H/<sup>18</sup>O ratios and a  
252 calibration curve of H<sub>2</sub>O (wt.%) vs. <sup>1</sup>H/<sup>18</sup>O determined using the 3 apatite standards with  
253 different H<sub>2</sub>O abundances (Fig. 2a). The curve was forced through the origin.

254 For the KREEP glass measurements, we used two basaltic glass standards (D52-5 and D51-  
255 3) with published D/H ratios (Hauri et al., 2002). The H<sub>2</sub>O contents of these two standards were  
256 determined by Rhea Workman using FTIR at Caltech. The H<sub>2</sub>O content of KREEP glass was  
257 calculated using a calibration curve (Fig. 2b) for H<sub>2</sub>O (wt.%) vs. <sup>1</sup>H/<sup>30</sup>Si. That curve was also  
258 forced through the origin. The reported errors on water contents and δD values include both  
259 the internal precision of an individual analysis and the external reproducibility (standard  
260 deviation) for standard measurements during a given analytical session.

261 The detection limit for H<sub>2</sub>O content was estimated by measuring nominally anhydrous  
262 minerals, such as olivine and pyroxene present in the same thin-sections, and a San Carlos  
263 olivine standard in a separate, epoxy-free standard mount. Samples were stored in a 60 °C  
264 vacuum oven to minimize the adsorption of water on section surfaces. As shown in Table 1,  
265 measurements with 2 nA primary beam resulted in a detection limit of ~ 100 ppm. The  
266 detection limit was later significantly improved by up to 10x by using a 4 nA primary beam. At  
267 least two things conspire to produce this improvement. First, a higher beam current increases  
268 the signal from the species that make up the sample, while the H from the vacuum system and  
269 that creeping along the sample surface remains approximately constant. Second, a higher  
270 beam current could more-efficiently remove surface H creeping in to the measurement area,  
271 thereby reducing the contaminant steady-state value. Yurimoto et al. (1989) and Stéphant and  
272 Robert (2014) also reported that use of higher primary beam current efficiently improves the  
273 detection limit of hydrogen measurement.

274 *3.1.2 The Open University (OU).* The Cameca NanoSIMS 50L was used for determining the  
275 H<sub>2</sub>O contents and H isotopic composition of apatites following the protocol described in details  
276 in Barnes et al. (2013, 2014a) and Tartèse et al. (2013). Polished samples were gold-coated for  
277 NanoSIMS analysis. A Cs<sup>+</sup> primary beam of ~ 260 pA current was used and negative secondary  
278 ions of <sup>1</sup>H, D, <sup>12</sup>C, and <sup>18</sup>O were collected simultaneously on electron multipliers. Electronic

279 gating was used to restrict counting secondary ions to the innermost 25 % of the sputtered  
280 area. Before analysis, pre-sputtering was performed over a 20  $\mu\text{m}$  x 20  $\mu\text{m}$  area using a  $\sim$  600  
281 pA primary beam for 1 minute to clean the sample surface and to locate the apatite using real  
282 time imaging (RTI), then further pre-sputtering was performed at a reduced area (analysis area)  
283 using the same beam conditions. An electron gun was used to provide charge compensation.  
284 Because of the variation in apatite grain size within and between samples, and the need to  
285 avoid cracks or inclusions, the analysis areas varied from 8  $\mu\text{m}$  x 8  $\mu\text{m}$  to 5  $\mu\text{m}$  x 5  $\mu\text{m}$ . The  
286 vacuum in the analysis chamber during analyses was  $\sim$  6.0 x 10<sup>-10</sup> Torr.

287 RTI was also carried out during the pre-sputtering to monitor <sup>1</sup>H and <sup>12</sup>C in order to identify  
288 cracks and hotspots. Occasionally, during an analysis a crack or hotspot appeared; in such a  
289 case, only the signal corresponding to analysis of the pristine sample was considered. This  
290 signal was isolated using the NanoSIMS DataEditor, software developed by Frank Gyngard  
291 (Washington University). Data inclusion was based on the <sup>12</sup>C signal, which is very low in lunar  
292 apatites but is several orders of magnitude higher for material filling the cracks (c.f. Barnes et  
293 al., 2014a; Tartèse et al., 2014).

294 Three terrestrial apatite standards (Ap003, Ap004, and Ap018 described in McCubbin et al.,  
295 2012) pressed in indium were used for calibration along with a “dry” San Carlos olivine crystal.  
296 This dry olivine was used to monitor instrumental background, which ranged between 13 and  
297 24 ppm H<sub>2</sub>O for the different analytical sessions. To ensure that this measure is adequate for  
298 epoxy-mounted samples, analyses were also carried out under routine analytical conditions in  
299 two plagioclase crystals in sample 15404. Two analyses of plagioclase yielded between 19 and  
300 33 ppm H<sub>2</sub>O, which is considered background H<sub>2</sub>O assuming that the crystals are indeed dry.  
301 Overall, the calculated background H<sub>2</sub>O contents for indium-pressed dry olivine and epoxy-  
302 mounted nominally anhydrous plagioclase were similar. Background H<sub>2</sub>O was then subtracted  
303 from the measured values of the unknown apatites.

304 *3.2. Galactic Cosmic Ray Exposure.*

305 Exposure to cosmic rays on the surface of the Moon can produce D and H *in situ*, which can  
306 alter the indigenous D/H ratio of lunar materials. Saal et al. (2013), Barnes et al. (2014a), and  
307 Robinson and Taylor (2014) demonstrated the importance of correcting for spallogenic D,  
308 especially in materials with low H<sub>2</sub>O content. Spallation-produced D will have a proportionally  
309 larger effect on the D/H ratio in samples with low water content than in samples with high  
310 water content (Saal et al. 2013) and for samples with long cosmic ray exposure ages. Since the  
311 apatites and glasses analyzed in this study have very low water contents (< 300 ppm H<sub>2</sub>O), this  
312 correction is important.

313 The measured data were corrected following the procedure of Saal et al. (2013), by  
314 determining the amount of spallation-produced D using the D production rate ( $4.6 \times 10^{-11}$   
315 mol/100 Myr, Merlivat et al., 1976) and the cosmic ray exposure (CRE) age of each sample, and  
316 then that contribution was subtracted from the measured D abundance for recalculating the  
317 D/H ratio. The reported uncertainty includes the uncertainty in the D production rate and the  
318  $2\sigma$  analytical uncertainties. The large uncertainty in the D production rate dominates the error  
319 of the corrected  $\delta D$  values ( $\sim 50\%$ , Saal et al. 2013). Unlike Saal et al. (2013), spallogenically  
320 produced H is not taken into account, because correcting for H has little effect on the overall  
321 D/H ratio. For example, the typical spallation correction for H expressed as H<sub>2</sub>O is only  $\sim 1$  ppm  
322 (Saal et al., 2013).

323 Cosmic ray exposure age data were available for samples 14321 (23.8 Ma, Lugmair and  
324 Marti, 1972; and 24 Ma, Burnett et al., 1972), 14161 (363 Ma, Kirsten et al., 1972), 76535 (195  
325 Ma, Bogard et al., 1975; 211 Ma, Crozaz et al., 1974; 233 Ma, Lugmair et al., 1976). When  
326 multiple ages were available, we averaged the ages. Since the error associated with the  
327 correction for cosmogenic D is dominated by the large uncertainty on the D production rate, we  
328 did not factor errors on the cosmic ray exposure ages into the total uncertainty of the corrected  
329 values. As the cosmic ray exposure (CRE) age of sample 15403/15404 has not been  
330 determined, the CRE age of  $11 \pm 1.1$  Ma for sample 15405 was used. Soil sample 15400 was  
331 collected from on top of 15405, and is classified as an immature soil.



332 Two samples, 77538 and 15358, have no CRE ages available. Sample 77538 was  
333 collected at Station 7 as a rake sample with lunar soil that was designated mature (Meyer,  
334 2015). According to Morris (1978), it takes 100 Ma of exposure time to develop a mature soil.  
335 Therefore, we take 100 Ma as the exposure age of 77538 for the purposes of spallogenic D  
336 correction, but this is only meant to be a rough estimate. Likewise, 15358 was collected as a  
337 rake sample from the rim of Spur Crater. Another KREEP basalt from the same rake sample,  
338 15382, has been CRE dated to 230 Ma (Stettler et al., 1973) and 240 Ma (Turner et al., 1973).  
339 We use the average of these two dates as an estimate for the CRE age of 15358.

340

#### 341 **4. Results**

342 Although we measure H, we report its concentration as H<sub>2</sub>O equivalent. In the lunar  
343 literature, “water” has been used to describe the presence of H, OH, or H<sub>2</sub>O collectively. As  
344 explained by Robinson and Taylor (2014), in magma “water” is present largely as OH until the  
345 total concentration reaches ~3.5 wt.%, at which point H<sub>2</sub>O becomes the dominant molecular  
346 species (Dixon et al., 1995). No lunar magmatic water concentrations reach such high levels,  
347 implying that it is present dominantly as OH. However, under the reducing conditions (e.g., IW-  
348 1) prevailing in lunar magmas, “water” probably consists of a combination of OH and H, with  
349 the proportion of H rising with increasing P and decreasing fO<sub>2</sub> (Elkins-Tanton and Grove, 2011;  
350 Hirschman et al., 2012, Sharp et al., 2013). To avoid confusion because of the uncertainty in  
351 how much of each species is present, we report our results as H<sub>2</sub>O equivalent. This approach is  
352 similar to reporting total Fe as FeO in electron microprobe analyses.

353 We performed analyses with the UH ims-1280 on a total of 18 points among 11 apatite  
354 grains from eight thin sections of intrusive rocks to determine their D/H ratios and water  
355 contents. We also made four measurements of residual glass in two KREEP basalt clasts in  
356 sample 15358,6 using the same instrument. Many apatite grains are too small (<30µm) or too  
357 cracked to be measured with the ims-1280, so they were analyzed with the NanoSIMS 50L ion  
358 microprobe at the Open University. A total of 19 points among 13 apatite grains from three  
359 thin sections were measured using the NanoSIMS. All of the δD values, water contents, and



360 their associated uncertainties are listed in Table 1. Apatite data are plotted on Fig. 3 and  
361 compared with literature apatite data in Fig. 4. Some of the data obtained with the ims-1280  
362 was first reported in Robinson et al. (2012, 2013) and Robinson and Taylor (2014).

363 The low H<sub>2</sub>O contents measured in KREEP-related materials (ranging from 23-267 ppm) is  
364 in stark contrast to apatite in most mare basalts, which contain ~1000-7500 ppm H<sub>2</sub>O (Fig. 4).  
365 One apatite in felsite 14321,1047 and two apatites in QMD 14161,7373 had H<sub>2</sub>O content below  
366 our detection limits. The KREEP basalt residual glass was similarly found to be water-poor,  
367 containing 58-95 ppm H<sub>2</sub>O with elevated  $\delta D$  value of +610 to +830 ‰ (Table 1).

368 The range in  $\delta D$  values for apatite in intrusive samples measured here is astoundingly large,  
369 varying from ultralow (-749 ‰) to quite elevated (+973 ‰). There are substantial uncertainties  
370 on the NanoSIMS measurements ( $2\sigma$  from 317-650‰) due to poor counting statistics when  
371 using relatively low probe currents, which are a result of low water abundances in the apatite,  
372 but these data are consistent with more precise measurements of apatite in the same sample  
373 (14321,1047 apt1) made with the ims-1280. Correction for spallogenic D decreases the  $\delta D$   
374 value by up to 184‰, yet many lunar apatites with detectable water show  $\delta D$  values higher  
375 than in the Earth's mantle, -218 to +60‰ (Boettcher et al., 1980; Michael 1998; Ahrens 1989;  
376 Deloule et al., 1991; Bell and Rossman 1992; Thompson 1992; Graham et al., 1994; Jambon  
377 1994; Wagner et al., 1996; Xia et al., 2002, Hallis et al., 2015). The  $\delta D$  values of other apatites  
378 fall near or somewhat below the terrestrial range. However, the  $\delta D$  of apatite in 15403,71 (as  
379 low as  $-749 \pm 56\%$ ) is by far the lightest  $\delta D$  value yet reported from the Moon, indicating that  
380 there could be a low D source in the lunar interior.

## 381 5. Discussion.

382 The data reported here and those previously published suggest that hydrogen isotopic  
383 compositions and possibly water concentrations vary widely in the lunar interior. Here we  
384 evaluate the extent of these apparent heterogeneities and the important implications these can  
385 have with regards to lunar formation and differentiation, and the accretion of volatiles to the  
386 lunar interior.

## 387 **5.1 Hydrogen isotopic composition: Multiple Reservoirs**

388 Apatites in this sample suite vary widely in  $\delta D$  value (Table 1, Fig. 3, 4), ranging from  $-754 \pm$   
389  $57 \text{ ‰}$  to  $+934 \pm 514 \text{ ‰}$  (spallation corrected). The  $\delta D$  values of apatites in individual samples  
390 (measured in this study and also in the literature) can also vary by 100s ‰ (Fig. 4). To evaluate  
391 broad variations among  $\delta D$  values and  $H_2O$  content of many samples, we made a histogram of  
392 the lowest D apatite analyses from each sample (Fig. 6). If degassing affected the H isotopic  
393 composition of a given sample, the lowest  $\delta D$  value will represent the least degassed  $\delta D$  for  
394 that sample. The data seem to cluster into groups with similar  $\delta D$  values. These clusters could  
395 represent different reservoirs in the lunar interior, which we evaluate below (Fig. 6).

### 396 *5.1.1. Earth-like reservoir.*

397 The range in  $\delta D$  value of Earth's present day upper mantle is estimated to be between -  
398  $-218$  and  $+60 \text{ ‰}$  (Boettcher et al. 1980; Michael 1998; Ahrens 1989; Deloule et al. 1991; Bell  
399 and Rossman 1992; Thompson 1992; Graham et al. 1994; Jambon 1994; Wagner et al. 1996; Xia  
400 et al. 2002; Hallis et al., 2015), shown by a line on Fig. 6. Several samples, including two KREEP  
401 basalts, five KREEP-rich intrusive rocks, and a mare basalt, fall in or near to this range in  $\delta D$   
402 values. As explained above, these KREEP-rich intrusive rocks formed at depth and pressure, so  
403 are less likely to have degassed and fractionated D from H prior to apatite crystallization. The  
404 rocks could thus retain their original (or close to their original) D/H ratios, which are essentially  
405 Earth-like (Barnes et al., 2014a). All of this evidence indicates that there is at least one  
406 reservoir in the lunar interior that has a  $\delta D$  value like the terrestrial mantle.

407 Despite the elevated  $\delta D$  values observed in mare basalt apatites, the mare basalt source may  
408 also be similar to the Earth-like  $\delta D$  reservoir. Calculations by Tartèse and Anand (2013) and  
409 Tartèse et al. (2013) showed that the entire range of elevated  $\delta D$  values observed in mare  
410 basalt apatite could be produced by degassing of 85-99% of the hydrogen from a melt with  
411 CI/CM-like chondritic  $\delta D$  signature of  $\sim +100 \text{ ‰}$ , (Alexander et al. 2012). While the water  
412 content of the mare basalts appears to be greater than the KREEPy intrusive rocks, they all  
413 could have had similar initial  $\delta D$  values, which are in or near the range of the terrestrial mantle.

414 Saal et al. (2013) and Furi et al. (2014) show that  $\delta D$  values of the pyroclastic glasses can be  
415 reconciled (after accounting for degassing) with being derived from a source region in the lunar  
416 interior with a  $\delta D$  value in the range of terrestrial rocks and carbonaceous chondrites. This is  
417 consistent with the isotopic compositions of olivine-hosted melt inclusions trapped within glass  
418 beads( Saal et al., 2013)

#### 419 *5.1.2. Moderately elevated D reservoir.*

420 Another cluster of analyses on Fig. 6 appears between  $\sim 150$ - $350$  ‰. Three of these samples  
421 are alkali suite rocks, formed intrusively through extensive fractional crystallization of KREEP  
422 basaltic magmas (Snyder et al., 1995). The alkali and Mg-suite rocks, however, formed  
423 intrusively and thus did not degas, or degassed little compared to eruptive samples. They could  
424 represent a reservoir inside the Moon with an inherent moderately elevated  $\delta D$  signature. It is  
425 also possible that these samples represent the high part of a range that begins with the  
426 terrestrial values, similar to those ( $\delta D +187$  to  $+327$  ‰) measured in melt inclusions by Saal et  
427 al., (2013), and so may not actually be resolvable from the Earth-like reservoir.

#### 428 *5.1.3. Low D reservoir.*

429 A distinct reservoir, with very low  $\delta D$  signature, is represented by apatites from samples  
430 15404,51, and -,55, and 15403,71. Apatite in these samples has an average  $\delta D$  value of  $-630$   
431 ‰, which is far below the range of the terrestrial mantle and of other  $\delta D$  values for apatites  
432 reported from the Moon (Fig. 4). REE abundances in 15404,36 (the parent chip of 15404,51 and  
433 -,55) are elevated with respect to those of Apollo 15 KREEP basalt (Lindstrom et al., 1992),  
434 which is consistent with formation from a KREEP basaltic magma, and its texture (exsolved  
435 pyroxene) indicates that it formed intrusively, thus avoiding H fractionation due to degassing.  
436 Even if the source of these Apollo 15 QMDs had degassed, degassing elevates  $\delta D$  values, which  
437 means that their source would have had an even lower initial  $\delta D$  value.

438 Solar wind is also extremely depleted in D ( $< -998$ ‰; Huss et al., 2012) and the range in  $\delta D$   
439 values of agglutinate glasses affected by solar wind from the regolith (Liu et al. 2012) is  
440 strikingly similar to the range seen in apatites from the Apollo 15 QMDs. However, there is no

441 clear mechanism for introducing solar wind H into fragments of intrusive rocks residing inside  
442 an impact melt. The Apollo 15 QMDs are considered to have formed at depth, in a shallow  
443 intrusion in the lunar crust (Ryder and Martinez, 1991), much deeper than D-depleted solar  
444 wind could have penetrated. Rock 15405, on which the 15403/4 regolith developed, is an  
445 impact melt breccia deposited at the site ca. 1.3 Ga ago. This boulder was probably formed and  
446 thrown to the Apollo 15 site by the impact event that formed Aristillus crater (Ryder 1976;  
447 Ryder and Martinez, 1991; Ryder et al., 1991; Taylor et al., 2012). It was subsequently buried  
448 and brought to the lunar surface at the Apollo 15 site only 11 Ma ago, based on its cosmic ray  
449 exposure age (Drozd et al., 1976). Direct implantation of solar wind H into these apatite grains  
450 is unlikely, as solar wind has been demonstrated to penetrate  $< 1 \mu\text{m}$  depth into the surface of  
451 a grain. Even if an apatite crystal was exposed directly on the surface the ambient lunar surface  
452 temperatures ( $\sim 100^\circ \text{C}$ ) are too low to allow significant diffusion of H into the crystal. Using  
453 data from Cherniak (2010) and the interdiffusion coefficient for OH, F, and Cl, the total diffusion  
454 distance is only  $\sim 10^{-5}$  microns at  $100^\circ \text{C}$  in 11 Ma.

455 In order for apatite in the Apollo 15 QMDs to be contaminated with solar wind, H from solar  
456 wind would have had to have been incorporated into their source impact melt breccia and  
457 subsequently diffused into the apatite grains. As discussed above, these samples were  
458 collected from on top of a three-meter boulder, sampled as 15405 (Meyer, 2015). Drozd et al.  
459 (1976) measured Ne, Kr, and Xe isotopes in 15405 and Bernatowicz et al. (1978) measured Ar  
460 isotopes in 15405 (matrix and a QMD clast) as part of their Ar-Ar dating. Both papers state that  
461 the rock contains no measurable solar wind component. Nevertheless, it is worth investigating  
462 whether enough regolith could be incorporated into the 15405 impact melt to impart a low  $\delta\text{D}$   
463 signature on the clasts in the rock.

464 Is it possible that the 15405 impact melt was contaminated with solar wind during its formation  
465 by the Aristillus impact? The pre-Aristillus regolith could have been a few meters thick, having  
466 formed between 3.8 Ga (the age of Imbrium) and 1.27 Ga (the age of Aristillus). We use 10 m  
467 for these calculations. How much of that 10 m layer would then be incorporated into the melt  
468 formed during the impact that produced Aristillus crater? Using equations 7.10.2 in Melosh

469 (1989) for a 55 km crater and assuming an impact velocity of 17 km/sec, a vertical impact angle,  
470 impactor density of  $3000 \text{ kg/m}^3$ , and target density of  $2500 \text{ kg/m}^3$ , we estimate that the  
471 projectile would have a radius of 1 km. The fraction of the impact melt derived from regolith is  
472 the regolith volume intersected by the footprint of the impacting projectile (1 km). Therefore,  
473 the regolith constitutes a disk 10 meters thick and 1 km in radius, equivalent to a volume of  
474  $0.031 \text{ km}^3$ . Dividing this by the total volume of the melt produced,  $500 \text{ km}^3$  (using projectile size  
475 and velocity noted above, after Grieve and Cintala 1992), gives a regolith fraction of 0.0063%. If  
476 the regolith contained 100 ppm H (close to the upper limit measured on Apollo regolith  
477 samples, Haskin and Warren, 1991), then the impact melt (assuming uniform mixing) would  
478 acquire 0.0063 ppm H. If all of the solar wind H was incorporated into apatite and the apatite  
479 abundance was 1% (the amount of normative apatite in KREEP basalt), then the apatite would  
480 contain a maximum of 0.6 ppm of solar wind derived H from the regolith atop the Aristillus  
481 target. This is equivalent to 5.4 ppm  $\text{H}_2\text{O}$ , which is only ~4% of the average water content of  
482 apatite in 15403, 71. Moreover, any solar wind H incorporated from the regolith would have  
483 then had to diffuse through the very rapidly cooling impact melt (Onorato et al., 1976) and rock  
484 fragments to eventually reach the apatite. We conclude that the low  $\delta\text{D}$  signature is not derived  
485 from solar wind contamination, but instead reflects the nature of the KREEP-rich rocks in the  
486 Aristillus target materials. This is supported by  $\delta\text{D}$  data from relict apatite grains in the impact  
487 melt of 15405 (Barnes et al., 2014b) that have preserved low  $\delta\text{D}$  values similar to those  
488 measured in 15403 and 15404 in this study.

489 The presence of a very low D reservoir in the lunar interior has interesting implications for  
490 potentially degassed samples with low  $\delta\text{D}$  values ( $\approx -100 \text{ ‰}$ ), such as the two basalts (NWA 773  
491 and 14053) that have  $\delta\text{D}$  signatures in the terrestrial range. Both of these samples have had  
492 their low  $\delta\text{D}$  values explained by lack of degassing (NWA 773, average  $\delta\text{D} \approx -29 \text{ ‰}$ , Tartèse et  
493 al., 2014) or incorporation of low D solar wind during impact heating (14053, average  $\delta\text{D} \approx -190$   
494  $\text{ ‰}$ , Greenwood et al., 2011). However, if a very low D reservoir existed in the Moon perhaps  
495 these samples owe their low  $\delta\text{D}$  signatures to a mantle source that was depleted in D. We  
496 calculate that if they had started with  $\delta\text{D}$  value of  $-500 \text{ ‰}$ , similar to the average  $\delta\text{D}$  value of  
497 15404,55, the average  $\delta\text{D}$  values of apatite in both 14053 and NWA 773 could be obtained with

498 > 85 % H<sub>2</sub> loss. This did not necessarily occur for these samples, but it is an intriguing  
499 possibility.

## 500 ***5.2 Heterogeneous water distribution in the lunar interior?***

501 The low H<sub>2</sub>O content (< 500 ppm) measured in the majority of KREEP-related materials  
502 is in stark contrast to the higher H<sub>2</sub>O contents (~1000-7500 ppm) of apatites in most mare  
503 basalts (Figs. 3, 4). Important exceptions are norites 77215 and 78235, and a granite clast in  
504 14303 (Barnes et al., 2014a). Despite attempts to calculate magmatic water contents from  
505 apatite data (McCubbin et al., 2010, Boyce et al., 2010, Barnes et al., 2013, Tartèse et al. 2013,  
506 2014, Robinson et al., 2013), Boyce et al. (2014) have shown that partitioning of OH, F, and Cl  
507 into apatite is complicated and depends on the relative and total abundances of these species,  
508 the timing of apatite crystallization, and the extent to which equilibrium was maintained during  
509 apatite crystallization of the melt. Estimating water content is further complicated by  
510 formation of late-stage melt pockets during crystallization in a lava flow (Pernet-Fisher et al.,  
511 2014).

512 While estimating the water content of a magma from apatite H<sub>2</sub>O might not be possible,  
513 the H<sub>2</sub>O concentration of residual glass in KREEP basalts in rock 15358 can be used to estimate  
514 the initial concentration in the magma before crystallization and loss occurred. The glass  
515 contains between 58 and 95 ppm H<sub>2</sub>O (Table 1) and represents the last ~20 % of melt  
516 remaining, as determined by modal analyses (Taylor et al., 2012). Because water is  
517 incompatible in all lunar minerals except apatite, its initial concentration in the magma would  
518 have increased as plagioclase and pyroxene crystallized. Thus, if no loss of H<sub>2</sub>O occurred, the  
519 parent magma would have contained 20% of the amount we measured in the glass, 12–19 ppm  
520 H<sub>2</sub>O. The relatively high  $\delta D$  value (average of +560 ‰, corrected for spallation) of the glass  
521 suggests that the magma might have lost water, as expected for a lava flow. To assess the initial  
522 water content, we calculated the amount of water loss by assuming that the initial  $\delta D$  value  
523 was -100 (earthlike) that loss was dominated by H<sub>2</sub>, and that the final  $\delta D$  is what we observe in  
524 the KREEP basalt clasts (+560 ‰), following the method used by Tartèse et al. (2013). The  
525 results are shown in Fig. 5. An initial  $\delta D$  value of -100 ‰ requires an initial H<sub>2</sub>O concentration of

526 115 ppm to produce the mean  $\delta D$  value of +560 ‰ and 85% loss of initial H. A lower initial  $\delta D$   
527 value would require a higher initial water content, but also a greater loss of H. Initial  $\delta D$   
528 equivalent to VSMOW implies an initial  $H_2O$  content of 80 ppm, requiring 80 % loss of the initial  
529 water to obtain a  $\delta D$  of 560 ‰. An initial  $\delta D$  signature of -500 ‰ (at the top of the range for  
530 the Apollo 15 QMDs), requires > 99.9 % water loss, which is unreasonable considering that the  
531 pyroclastic glasses lost only about 98% (Saal et al., 2008).

532 These estimates lead us to conclude that the lava in which the KREEP basalt clasts in  
533 15358 formed could have had an Earth-like initial  $\delta D$  signature ( $\sim 0$  ‰) and  $\sim 100$  ppm  $H_2O$ . For  
534 comparison, melt inclusions in olivine in Apollo 17 orange glass beads (Hauri et al., 2011; Saal et  
535 al., 2013) contain 270–1200 ppm. Assuming that lower values reflect H loss from the inclusions,  
536 we infer that the orange glass magma contained  $\sim 1000$  ppm  $H_2O$ , about an order of magnitude  
537 larger than we estimate for the KREEP basalts in 15358. Saal et al. (2008) calculated from  
538 diffusion profiles of H, Cl, F, and S that the pre-eruption magma for the VLT glass contained  
539 260–745 ppm  $H_2O$ , consistent with melt inclusion measurements in the orange glass. Assuming  
540 10% partial melting, the mantle sources for the orange glass, green glass, and KREEP basalt  
541 magmas would have contained 100 ppm, 75 ppm, and 10 ppm  $H_2O$ , respectively, suggesting a  
542 range in mantle  $H_2O$  contents. Clearly, more work on KREEP basalts and KREEP-rich glasses is  
543 needed in order to fully understand the relationship between glass/melt inclusion  $H_2O$  content  
544 and source region water content.

545

### 546 ***5.3 Implications for the lunar interior.***

547 The primary goal of all measurements of water in volcanic glasses, melt inclusions, and  
548 apatites is to determine the bulk water content and sources of water in the Moon. The  
549 observed heterogeneities in water abundance and  $\delta D$  values in the lunar interior present a  
550 major problem, as it is unclear which samples, if any, are the most representative of the Moon  
551 as a whole. The most reliable  $H_2O$  abundance measurements for determining pre-eruptive  
552 water content of lunar magmas come from the melt inclusions in olivine in pyroclastic glass



553 beads, which indicates that at least one part of the lunar interior contains as much water as the  
554 source regions of MORBs (Hauri et al., 2011). These melt inclusions did not lose much water  
555 when they formed, which means their  $\delta D$  values are minimally fractionated (Saal et al., 2013).  
556 After correction for spallation, the  $\delta D$  values of the A17 melt inclusions range from +187 to  
557 +327 ‰ (Saal et al., 2013). To the extent that H loss did happen, the original  $\delta D$  would have  
558 been lower. This is near the Earth range, but it is also near the range of the moderately-  
559 enriched  $\delta D$  value reservoir discussed above, which primarily consists of KREEP-rich, intrusive  
560 rocks. This may also indicate that the moderately enriched reservoir could be related to the  
561 Earthlike reservoir.

562 Fri et al., (2014) reported data suggesting that the source of the Apollo 17 orange glass  
563 (74002) had an initial  $\delta D$  value of  $-100$  ‰, which is within the range of the terrestrial mantle.  
564 Does this suggest a common source of water in the terrestrial mantle and some portions of the  
565 lunar interior? Fri et al., (2014) point out that a  $\delta D$  value of  $-100$  ‰ is within the range of  
566 carbonaceous chondrites, and could indicate the delivery of at least some water to the Earth-  
567 Moon system by late accretion (e.g., Saal et al., 2013; Tartse and Anand 2013; Tartse et al.,  
568 2013; Tartse et al., 2014). However, if this water was not added after lunar formation to the  
569 Earth-Moon system, then it could be conceived that water was retained during the Giant  
570 Impact event allowing for some regions to contain substantial water, with Earth-like  $\delta D$   
571 signature (Saal et al., 2013; Barnes et al., 2014a; Fri et al., 2014).

572 Greenwood et al. (2011) were the first to measure  $\delta D$  signatures of apatite in lunar samples,  
573 and they showed that apatite in mare basalts were characterized by elevated  $\delta D$  values ( $> 800$   
574 ‰). They suggested that the Moon accreted dry (constrained by Moon-formation-evolution  
575 models available at the time), and water was added later from a source, such as comets,  
576 already characterized by water with high  $\delta D$  values. This seems unlikely. The mare basalts  
577 almost certainly lost water when erupted, so their  $\delta D$  values are elevated by the process of  
578 magmatic degassing of  $H_2$  which preferentially fractionates H over D isotopes (as discussed in  
579 the previous sections). Tartse and Anand (2013) calculated that pre-eruptive mare basalt  
580 magmas could have been characterized by  $\delta D$  values of  $\sim 100$  ‰, but lost 85-99 % of their



581 water, which consequently elevated the  $\delta D$  value of the water. Thus, there is no compelling  
582 need for a source with high  $\delta D$  values in the lunar interior. It is possible that late-delivered  
583 volatiles could have been added after the mantle cumulates were formed but prior to the  
584 formation of a significantly thick crust (e.g., Hauri et al., 2015).

585 The apparently dry regions of the lunar interior vary in  $\delta D$  values from moderately  
586 enriched to extremely depleted. The regions that are moderately enriched compared to Earth  
587 may reflect fractionation in the proto-lunar disk after the Moon-forming impact (Desch and  
588 Taylor, 2012; Hauri et al., 2015). Fractionation of D from H (preferential loss of lighter H) is  
589 consistent with the presence of heavy Zn isotopic signatures in lunar samples (Paniello et al.,  
590 2012). H loss from the disk needs to be modelled thoroughly, but if H loss was high ( $\sim 90\%$ )  
591 during lunar formation, D/H fractionation could have been sufficient to change the  $\delta D$  value  
592 from  $-218\text{‰}$  (the lower range of terrestrial mantle values) to the range shown by the  
593 moderately enriched lunar reservoir ( $+200$  to  $+400\text{‰}$ ). Alternatively, the potentially dry  
594 regions of the lunar interior with  $\delta D$  values in the terrestrial range might reflect Moon-forming  
595 materials that lost water, but did not fractionate D from H. The regions with Earth-like  $\delta D$   
596 signatures could also have formed by extensive fractionation of H from D during lunar  
597 formation, but began with a low  $\delta D$  values like those observed in Apollo 15 QMD apatites. This  
598 implies that the primitive Earth could have had a much lower  $\delta D$  signature than is currently  
599 considered for the present-day upper mantle. In fact, primitive mantle sources have been  
600 identified and at least some contain low  $\delta D$  values, as low as  $-218 \pm 34\text{‰}$  (Hallis et al., 2015).  
601 Halliday (2013) explains the Earth's low  $\delta D$  as a mixture of chondritic and solar components.

602 Our study has contributed to the growing dataset for water and H-isotopes from lunar  
603 apatites, and has targeted mostly intrusive rocks of the lunar highlands (felsites and QMDs).  
604 The data presented are in agreement with previous work advocating for the heterogeneous  
605 distribution of water in the lunar interior (e.g., Anand, 2010; McCubbin et al., 2011; Robinson  
606 and Taylor, 2014). The apatites in Apollo 15 QMDs record a water reservoir in the lunar interior  
607 that is characterized by an anomalously low D/H ratio ( $\sim -600\text{‰}$ ), the lowest yet recorded for  
608 the lunar interior. This is distinct from the majority of lunar samples, which range in  $\delta D$  values

609 of -200 to +100 ‰ compatible with results from lunar highlands cumulates, mare and KREEP  
610 basalts, and picritic glasses (Saal et al., 2013; Füri et al., 2014; Barnes et al., 2014a; Tartèse et  
611 al., 2014), though some samples have  $\delta D$  values as high as +600 to +700 ‰. The origin or  
612 source of this uniquely D-depleted reservoir is ambiguous but could be an isotopic signature  
613 resulting from Moon formation through fractionation of H isotopes in the protolunar disk, the  
614 incorporation of a primitive Solar component to the lunar interior, or a signature inherited from  
615 a depleted reservoir in the proto-Earth.

## 616 **Summary and Conclusions.**

617 The measurements of KREEP-rich intrusive samples presented here, along with  
618 literature data, show that apatite in the KREEP-rich intrusive rocks is low in H<sub>2</sub>O. Though  
619 apatite cannot be used to calculate pre-eruptive magmatic water content, our measurements  
620 of residual glass in KREEP basalt fragments in 15358 suggest that the KREEP-basaltic parent  
621 magmas to the felsites and QMDs was very dry, with the mantle source of 15358 containing  
622 ~10 ppm H<sub>2</sub>O, about ten times less than the mantle source of the A17 pyroclastic glasses. This  
623 suggests at least two different reservoirs for water in the lunar mantle; one “wet” and one  
624 “dry”, which complicates determining the bulk water content of the Moon.

625 In addition to the water content of apatite in these KREEP-rich intrusive rocks, we have  
626 also measured their H isotope compositions and compared them with literature data. Lunar  
627 apatites show an astonishingly large range in  $\delta D$  and may fall into a number of reservoirs.  
628 Many lunar rocks, including the mare basalts, seem to have had initial  $\delta D$  similar to that of  
629 Earth’s mantle, while the drier KREEP-rich rocks studied here are moderately elevated in D with  
630 respect to Earth. The most surprising results came from apatite in Apollo 15 QMDs 15404, 51,  
631 15404,55, and 15403, 71, which have the lowest  $\delta D$  measured in lunar apatite so far, as low as -  
632 754 ‰. These QMDs may represent another reservoir in the lunar mantle that could preserve a  
633 primitive, D-depleted component within the Moon, perhaps inherited from the proto-Earth.

634 Our data indicate that water is heterogeneously distributed in the Moon, varying in both  
635 concentration and hydrogen isotopic composition. How these distinctive reservoirs formed is

636 unclear, but likely reflect a combination of lunar formation and differentiation. Bulk lunar water  
637 concentration is difficult to constrain, but the variability in water content and D/H may be much  
638 more informative about lunar origin than is the total amount of water in the Moon.

639

640 **Acknowledgements.** The authors thank Romain Tartèse for his assistance in collecting data  
641 and for highly useful discussions. This research was supported by the National Aeronautics and  
642 Space Administration through the NASA Astrobiology Institute under Cooperative Agreement  
643 No. NNA09DA77A issued through the Office of Space Science, by NASA Lunar Advanced Science  
644 and Exploration Research Grant NNX11AE85G, the Solar System Exploration Research Virtual  
645 Institute (through the Center for Lunar Science and Exploration cooperative agreement  
646 NNA14AB07A, David Kring, PI), and by The Bullard Foundation. STFC are also thanked for a PhD  
647 studentship to JJB and research grants to MA (Grant no. ST/I001298/1 and ST/L000776/1). We  
648 thank three anonymous reviewers and associate editor Alexander Nemchin for insightful and  
649 critical comments that helped improve the quality of the manuscript.

650

651

652

### 653 **References.**

654 Ahrens, T. J. (1989) Water storage in the upper mantle. *Nature* **342**, 122–123.

655 Alexander, C. M. O'D. et al. (2012) The provenances of asteroids, and their contributions to the  
656 volatile inventories of the terrestrial planets, *Science* **337**, 721-723, doi:  
657 10.1126/science.1223474.

658 Anand M. (2010) Lunar water: a brief review. *Earth Moon Planet.* **107**, 65–73.

659 Aubaud C., Hauri E. H., and Hirshmann M. M. (2004) Water partitioning coefficients between  
660 nominally anhydrous minerals and basaltic melts. *Geophys. Res. Lett.* **31**, doi  
661 10.1029/2004GRL021341.

662 Barnes J.J., Franchi I.A., Anand M., Tartèse R., Starkey N.A., Koike M., Sano Y., Russell S.S. (2013)  
663 Accurate and precise measurements of the D/H ratio and hydroxyl content in lunar apatites  
664 using NanoSIMS. *Chem. Geo.* **337-338**, 48-55.

- 665 Barnes J.J., Tartèse R., Anand M., McCubbin F.M., Franchi I.A., Starkey N.A., and Russell S.S.  
666 (2014a) The origin of water in the primitive Moon as revealed by the lunar highlands  
667 samples. *Earth Planet. Sci. Lett.* **390**, 244-252.
- 668 Barnes J.J., Tartèse R., Anand M., McCubbin F.M., Franchi I.A., Starkey N.A., and Russell S.S.  
669 (2014b) The hydrogen isotopic composition of apatites in lunar impact-melt breccias. *Lunar*  
670 *Planet. Sci. XLV*. Lunar Planet. Inst., Houston. #1978 (abstr.).  
671
- 672 Bell, D. R. & Rossman, G. R. (1992) Water in Earth's mantle: the role of nominally anhydrous  
673 minerals. *Science* **255**, 1391–1396.
- 674 Bernatowicz T.J., Hohenberg C.M., Hudson B., Kennedy B.M. and Podosek F. (1978) Argon ages  
675 for lunar breccias 14064 and 15405. *Proc. 9<sup>th</sup> Lunar Planet. Sci. Conf.*, 905-919.  
676
- 677 Boettcher A. L. and O'Neil J. R. (1980) Stable isotope, chemical and petrographic studies of high  
678 pressure amphiboles and micas: evidence for metasomatism in the mantle source regions  
679 of alkali basalts and kimberlites. *Am. J. Sci.* **280A**, 594–621.
- 680 Bogard D.D., Nyquist L.E., Bansal B.M., Wiesmann H. and Shih C.-Y. (1975) 76535: An old lunar  
681 rock. *Earth Planet. Sci. Lett.* **26**, 69-80.  
682
- 683 Boyce J. W., Tomlinson S. M., McCubbin F. M., Greenwood J. P., and Treiman A. H. (2014) The  
684 lunar apatite paradox. *Science Express* 20 March 2014 [10.1126/science.1250398](https://doi.org/10.1126/science.1250398)
- 685 Boyce J.W., Liu Y., Rossman G.R., Guan Y., Eiler J.M., Stolper E.M., and Taylor L.A. (2010) Lunar  
686 apatite with terrestrial volatile abundances. *Nature* **466**, 466-469.
- 687 Bucholz C. E., Gaetani G.A., Behn M.D., and Shimizu N. (2013) Post-entrapment modification of  
688 volatiles and oxygen fugacity in olivine-hosted melt inclusions. *Earth Planet. Sci. Lett.* **374**,  
689 145-155.
- 690 Burnett D.S., Huneke J.C., Podosek F.A., Russ G.P., Turner G. and Wasserburg G.J. (1972) The  
691 irradiation history of lunar samples. *Lunar Sci. III.*, Lunar Inst., Houston, 105-107 (abstr.)  
692
- 693 Cherniak D.J. (2010) Diffusion in accessory minerals: zircon, titanite, apatite, monazite and  
694 xenotime. *Rev. Mineral. Geochem.*, **72**, 827-869.  
695
- 696 Crozaz G., Drozd R., Hohenberg C., Morgan C., Ralston C., Walker R. and Yuhas D. (1974) Lunar  
697 surface dynamics: Some general conclusions and new results from Apollo 16 and 17. *Proc.*  
698 *5<sup>th</sup> Lunar Sci. Conf.*, 2475-2499.  
699
- 700 Deloule E., Albarède F. and Sheppard S. M. F. (1991) Hydrogen isotope heterogeneities in the  
701 mantle from ion probe analysis of amphiboles from ultramafic rocks. *Earth. Planet. Sci.*  
702 *Lett.* **105**, 543–553.

- 703  
704 Desch S.J. and Taylor G. J. (2012) Volatile depletion from the protolunar disk. *Euro. Planet. Sci.*  
705 *Cong. 7*, Abst.# 272.
- 706 Dixon J.E., Stolper E. M., and Holloway J.R. (1995) An experimental study of water and carbon  
707 dioxide solubilities in mid-ocean ridge basaltic liquids: I. Calibration and solubility models.  
708 *Jour. Petrology* **36**, 1607-1631.
- 709 Drozd R.J., Kennedy B.M., Morgan C.J., Podosek F.A. and Taylor G.J. (1976) The excess fission  
710 Xenon problem in lunar samples. *Proc. 7<sup>th</sup> Lunar Sci. Conf.*, 599-623.  
711
- 712 Dymek R. F., Albee A. L. and Chodos A. A. (1975) Comparative petrology of lunar cumulate rocks  
713 of possible primary origin: Dunite 72415, troctolite 76535, norite 78235, and anorthosite  
714 62237. *Proc. 6<sup>th</sup> Lunar Sci. Conf.* 301-341.
- 715 Elardo S. M., McCubbin F. M. and Shearer C. K. Jr. (2012) Chromite symplectites in Mg-suite  
716 troctolite 76535 as evidence for infiltration metasomatism of a lunar layered intrusion.  
717 *Geochim. Cosmochim. Acta* **87**, 154-17.
- 718 Elardo S. M., Draper D. S. and Shearer C. K. Jr. (2011) Lunar Magma Ocean crystallization  
719 revisited: Bulk composition, early cumulate mineralogy, and the source regions of the  
720 highlands Mg-suite. *Geochim. Cosmochim. Acta* **75**, 3024-3045.
- 721 Elkins-Tanton L. T. and Grove T.L. (2011) Water (hydrogen) in the lunar mantle: Results from  
722 petrology and magma ocean modelling. *Earth Planet. Sci. Lett.* **307**, 173-179.
- 723 Füri E., Deloule E., Gurenko A. and Marty B. (2014) New evidence for chondritic lunar water  
724 from combined D/H and noble gas analyses of single Apollo 17 volcanic glasses. *Icarus* **229**,  
725 109-120.
- 726 Gaetani G.A., O'Leary J.A., Shimizu N., Bucholz C.E. and Newville M., (2012) Rapid re-  
727 equilibration of water and oxygen fugacity in olivine-hosted melt inclusions. *Geology* **40**,  
728 915-918.
- 729 Geiss J. and Gloecker G. (1998) Abundances of Deuterium and Helium-3 in the protosolar cloud.  
730 *Space Sci. Rev.* **84**, 239-250.
- 731 Gooley R.C., Brett R., Warner J.L. and Smyth J.R. (1974) A lunar rock of deep crustal origin:  
732 Sample 76535. *Geochim. Cosmochim. Acta* **38**, 1329-1339.
- 733 Grant K. J., Kohn S. C., and Brooker R. A. (2007) The partitioning of water between olivine,  
734 orthopyroxene and melt synthesized in the system albite-forsterite-H<sub>2</sub>O. *Earth Planet. Sci.*  
735 *Lett.* **260**, 227-241.

- 736 Graham C., Kinny P., Harte B. and Valley J. (1994) The nature and scale of stable isotope  
737 disequilibrium in the mantle: ion and laser microprobe evidence. *Mineral. Mag.* **58A**, 345–  
738 346.
- 739 Greenwood J. P., Itoh S., Sakamoto N., Warren P., Taylor L. and Yurimoto H. (2011) Hydrogen  
740 isotope ratios in lunar rocks indicate delivery of cometary water to the Moon. *Nature*  
741 *Geosci.* **4**, 79-82.
- 742 Grieve R. A. F. and Cintala M. J. (1992) An analysis of differential impact melt-crater scaling and  
743 implications for the terrestrial impact record. *Meteoritics* **27**, 526-538.
- 744  
745 Halliday A. N. (2013) The origins of volatiles in the terrestrial planets. *Geochim. Cosmochim.*  
746 *Acta* **105**, 146-171.
- 747 Hallis L. J., Huss G. R., Nagashima K., Taylor G. J., Halldórsson S. A., Hilton D.R., Mottl M. J. and  
748 Meech K. J. (2015) Evidence for primordial water in Earth's deep mantle. *Science* **350**, 795-  
749 797.
- 750 Hallis L. J., Taylor G. J., Nagashima K. and Huss G. R. (2012) Magmatic water in the martian  
751 meteorite Nakhla. *Earth Planet. Sci. Lett.* **359-360**, 84-92.
- 752 Harrison T.M., and Watson E.B. (1984) The behavior of apatite during crustal anatexis: Equilib-  
753 rium and kinetic considerations: *Geochim. Cosmochim. Acta* **48**, 1467-1477.
- 754 Haskin L. and Warren P. (1991) Lunar chemistry. In *Lunar Sourcebook: a user's guide to the*  
755 *Moon*, eds. G. H. Heiken, D. T. Vaniman, and B. M. French. Cambridge University Press, pp.  
756 357-474.
- 757 Hauri E. (2002) SIMS analysis of volatiles in silicate glasses, 2: isotopes and abundances in  
758 Hawaiian melt inclusions. *Chem. Geol.* **183**, 115-141.
- 759 Hauri E. H., Weinreich T., Saal A. E., Rutherford M. C. and Van Orman J. A. (2011) High pre-  
760 eruptive water contents preserved in lunar melt inclusions. *Science* **333**, 213-215.
- 761 Hauri E., Wang J., Dixon J.E., King P.L., Mandeville C. and Newman S. (2002). SIMS analysis of  
762 volatiles in silicate glasses 1. Calibration, matrix effects and comparisons with FTIR. *Chem.*  
763 *Geol.* **183**, 99-114.
- 764 Hauri, E., Saal, A. E., Rutherford, M. J. and Van Orman, J. A. (2015) Water in the Moon's interior:  
765 Truth and consequences. *Earth Planet. Sci. Lett.* **409**, 252-264.
- 766 Hess P. C., Rutherford M. J., Guillemette R. N., Ryerson F. J. and Tuchfeld H. A. (1975) Residual  
767 products of fractional crystallization of lunar magmas: An experimental study. *Proc. 6<sup>th</sup>*  
768 *Lunar Sci. Conf.*, 895-909.

- 769 Hess P.C., Rutherford M.J. and Campbell H.W. (1978) Ilmenite crystallization in nonmare basalt:  
770 Genesis of KREEP and high-Ti mare basalt. *Proc. 9<sup>th</sup> Lunar Sci. Conf.* 705-724.
- 771 Hess P.C., Horezmpa P. and Rutherford M. J. (1989) Fractionation of Apollo 15 KREEP basalts.  
772 *20<sup>th</sup> Lunar Planet. Sci.*, Lunar Planet Inst., Houston, #1209 (abstr.).
- 773 Hirschmann M. M., Wirthers A. C., Ardia P. and Foley (2012) N. T. Solubility of molecular  
774 hydrogen in silicate melts and consequences for volatile evolution of terrestrial planets.  
775 *Earth Planet. Sci. Lett.* **345-348**, 38-48.
- 776 Hughes J. M., Jolliff B. L. and Rakovan J. (2008) The crystal chemistry of whitlockite and  
777 merrillite and the dehydrogenation of whitlockite to merrillite. *Amer. Mineral.* **93**, 1300-  
778 1305.
- 779 Huss G. R., Nagashima K., Burnett D. S., Jurewicz A. J. G. and Olinger C. T. (2012) A new upper  
780 limit on the D/H ratio in the solar wind. *Lunar Planet. Sci. XLIII*, Lunar Planet. Inst.,  
781 Houston, #1709 (abstr.).
- 782 Jambon, A. (1994) Earth degassing and large-scale geochemical cycling of volatile elements. In  
783 *Volatiles in Magmas* (eds. M. R. Carroll and J. R. Holloway), *Rev. Mineralogy* **30**  
784 Mineralogical Society of America. pp. 479–517.
- 785 Jolliff B.L. (1991) Fragments of quartz monzodiorite and felsite in Apollo 14 soil particles. *Proc.*  
786 *21<sup>st</sup> Lunar Planet. Sci. Conf.*, 101-118.
- 787 Jolliff B. L., Floss C., McCallum I. S. and Schwartz J. M. (1999) Geochemistry, petrology, and  
788 cooling history of 14161,7373: A plutonic lunar sample with textural evidence of granitic-  
789 fraction separation by silicate-liquid immiscibility. *Amer. Mineral.* **84**, 821-837.
- 790 Jolliff B. L., Hughes, J.M., Freeman, J. J. and Zeigler R. A. (2006) Crystal chemistry of lunar  
791 merrillite and comparison to other meteoritic and planetary suites of whitlockite and  
792 merrillite. *Am. Min.*, **91**, 1583-1595.  
793
- 794 Kirsten T., Deubner J., Horn P., Kaneoka I., Kiko J., Schaeffer O.A. and Thio S.K. (1972) The rare  
795 gas record of Apollo 14 and 15 samples. *Proc. 3<sup>rd</sup> Lunar Sci. Conf.*, 1865-1889.  
796
- 797 Koga K., Hauri E., Hirshmann M. and Bell D. (2003) Hydrogen concentration analyses using SIMS  
798 and FTIR: comparison and calibration for nominally anhydrous minerals. *Geochem.*  
799 *Geophys. Geosys.* **4**, 1019, doi: 10.1029/2002GC000378.
- 800 Lindstrom M. M., Mittlefehldt D.W., and Martinez R.R. (1992) Geochemical studies of Apennine  
801 Front coarse-fines particles. *23<sup>rd</sup> Lunar Planet Sci.*, Lunar Planet. Inst., Houston, #1388  
802 (abstr).



- 803 Liu Y., Guan Y., Zhang Y., Rossman G. R., Eiler J. M. and Taylor L.A. (2012) Direct measurement  
804 of hydroxyl in the lunar regolith and the origin of lunar surface water. *Nature Geosci.* **5**:  
805 779-782.
- 806 Lugmair G. W. and Marti K. (1972) Exposure ages and neutron capture record in lunar samples  
807 from Fra Mauro. *Proc. 3<sup>rd</sup> Lunar Sci. Conf.*, 1891-1897.  
808
- 809 Lugmair G. W., Marti K., Kurtz J. P. and Scheinin N. B. (1976) History and genesis of lunar  
810 troctolite 76535 or: How old is old? *Proc. 7<sup>th</sup> Lunar Sci. Conf.* 2009-2033.
- 811 Marvin U. B., Lindstrom M. M., Holmberg B. B. and Martinez R. R. (1991) New observations on  
812 the quartz monzodiorite-granite suite. *Proc. 21<sup>st</sup> Lunar Planet. Sci. Conf.*, 119-135.
- 813 McCallum, I. S., Domeneghetti, M. C., Schwartz, J. M., Mullen, E. K., Zema, M., Cámara, F.,  
814 McCammon, C. and Ganguly, J. (2006) Cooling history of lunar Mg-suite gabbro-norite  
815 76255, troctolite 76535 and Stillwater pyroxenite SC-936: The record in exsolution and  
816 ordering in pyroxenes. *Geochim. Cosmochim. Acta* **70**, 6068-6078.
- 817 McCubbin F. M., Steele A., Hauri E. H., Nekvasil H., Yamashita S. and Hemley R. J. (2010)  
818 Nominally hydrous magmatism on the Moon. *Proc. Natl. Acad. Sci. USA* **107**, 11223-11228.
- 819 McCubbin F. M., Jolliff B. J., Nekvasil H., Carpenter P. K., Zeigler R. A., Steele A., Elardo S. M. and  
820 Lindsley D. H. (2011) Fluorine and chlorine abundances in lunar apatite: Implications for  
821 heterogeneous distributions of magmatic volatiles in the lunar interior. *Geochim.*  
822 *Cosmochim. Acta* **75**, 5073-5093.
- 823 McCubbin F. M., Hauri E. H., Elardo S. M., Vander Kaaden K. E., Wang, J. and Shearer C. K.,  
824 (2012). Hydrous melting of the martian mantle produced both depleted and enriched  
825 shergottites. *Geology* **40**, 683-686.  
826
- 827 McCubbin, F. M., Shearer, C. K., Burger, P. V., Hauri, E. H., Wang, J., Elardo, S. M., & Papike, J. J.  
828 (2014). Volatile abundances of coexisting merrillite and apatite in the martian meteorite  
829 Shergotty: Implications for merrillite in hydrous magmas. *Amer. Mineral.* **99**, 1347-1354.  
830
- 831 Melosh H. J. (1989) *Impact Cratering: A Geologic Process*. Oxford University Press, New York.  
832 245 pp.  
833
- 834 Merlivat, L., Leiu, M., Neif, G. and Roth, E. (1976) Spallation deuterium in rock 70215. *Proc.*  
835 *Lunar Sci. Conf. 7th*, 649-658.  
836
- 837 Meyer C. (2015) The Lunar Sample Compendium. <http://curator.jsc.nasa.gov/lunar/lsc/>  
838
- 839 Michael P. J. (1988) The concentration, behavior and storage of H<sub>2</sub>O in the suboceanic upper  
840 mantle: implications for mantle metasomatism. *Geochim. Cosmochim. Acta* **52**, 555-566.  
841



- 842 Morris R.V. (1978) The surface exposure (maturity) of lunar soils; some concepts and I<sub>2</sub>/FeO  
843 compilation. *Proc. 9<sup>th</sup> Lunar Planet. Sci.* 2287-2297.
- 844 Newman S. and Lowenstern J.B. (2002) VolatileCalc: a silicate melt-H<sub>2</sub>O-CO<sub>2</sub> solution model  
845 written in Visual Basic for Excel. *Comp. and Geosci.* **28**, 597-604).
- 846 Onorato P. I. K., Uhlmann D. R., and Simonds C. H. (1976) Heat flow in impact melts: Apollo 17  
847 station 6 boulder and some applications to other breccias and xenolith laden melts. *Proc.*  
848 *Lunar Sci. Conf. 7<sup>th</sup>*, 2429-2467.
- 849 Paniello R. C., Day J. M. D. and Moynier F. (2012) Zinc isotopic evidence for the origin of the  
850 Moon. *Nature* **490**, 376-379.
- 851 Pernet-Fisher J. F., Howarth G. H., Liu Y., Chen Y. and Taylor L. A. (2014) Estimating the lunar  
852 mantle water budget from phosphates: Complications associated with silicate-liquid-  
853 immiscibility. *Geochim. Cosmochim. Acta* **144**, 326-341.
- 854 Robinson K. L. and Taylor G. J. (2011) Intrusive and extrusive lunar felsites. *42<sup>nd</sup> Lunar Planet*  
855 *Sci.*, Lunar Planet Inst., Houston, #1257 (abstr).
- 856 Robinson K. L. and Taylor G. J. (2014) Heterogeneous distribution of water in the Moon. *Nature*  
857 *Geosci.* **7**, 401-408.
- 858 Robinson K. L., Hellebrand E. and Taylor G. J. (2015) The physical setting for felsite formation.  
859 *46<sup>th</sup> Lunar Planet Sci.*, Lunar Planet. Inst., Houston, #1623 (abstr.).
- 860 Robinson K. L., Taylor G. J. and Nagashima K. (2013) D/H of intrusive moon rocks: Implications  
861 for lunar origin. *Lunar Planet Sci. XLIV*, Lunar Planet. Inst., Houston, #1327 (abstr.).
- 862 Robinson K. L., Taylor G. J., Hellebrand E. and Nagashima K. (2012) Water in evolved lunar rocks:  
863 Implications for water distribution in the lunar mantle. *Lunar Planet Sci. XLIII*, Lunar Planet.  
864 Inst., Houston, #1727 (abstr.).
- 865 Roedder E. and Weiblen P. W. (1971) Petrology of silicate melt inclusions, Apollo 11 and Apollo  
866 12 and terrestrial equivalents. *Proc. 2<sup>nd</sup> Lunar Sci. Conf.*, 507-528.
- 867 Rutherford M. J., Hess P. C. and Daniel G. H. (1974) Experimental liquid line of descent and  
868 liquid immiscibility for basalt 70017. *Proc. 5<sup>th</sup> Lunar Sci. Conf.*, 569-583.
- 869 Ryder G. (1976) Lunar sample 15405: Remnant of a KREEP basalt-granite differentiated pluton.  
870 *Earth Planet. Sci. Lett.* **29**, 255-268.
- 871 Ryder G. (1988) Quenching and disruption of lunar KREEP lava flows by impacts. *Nature* **336**,  
872 751-754.
- 873 Ryder G. and Martinez R. R. (1991) Evolved hypabyssal rocks from station 7, Apennine Front,  
874 Apollo 15. *Proc. 21<sup>st</sup> Lunar Planet. Sci. Conf.*, 137-150.

- 875 Ryder G., Bogard D. and Garrison D. (1991) Probable age of Autolyucus and calibration of lunar  
876 stratigraphy. *Geology* **19**, 143–146.
- 877 Ryder G., Stoesser D. B., Marvin U. B. and Bower J. F. (1975) Lunar granites with unique ternary  
878 feldspars. *Proc. 6<sup>th</sup> Lunar Planet. Sci. Conf.*, 435-449.
- 879 Saal A. E., Hauri E. H., Lo Cascio M., Van Orman J. A., Rutherford M. C. and Cooper R.F. (2008)  
880 Volatile content of lunar volcanic glasses and the presence of water in the Moon's interior.  
881 *Nature* **454**, 192-195.
- 882 Saal A. E., Hauri E. H., Van Orman J. A. and Rutherford M. J. (2013) Hydrogen isotopes in lunar  
883 volcanic glasses and melt inclusions reveal a carbonaceous chondrite heritage. *Science*  
884 **340**, 1317-1320.
- 885 Schwartz J. M. and McCallum I. S. (1999) Inferred depths of formation of spinel cataclasites and  
886 troctolitic granulite, 76535 using new thermodynamic data for Cr-spinel. *Lunar Planet.*  
887 *Sci. XXX*, Lunar Planetary Institute, Houston, #1308 (abstr.).
- 888 Sharp Z. D., McCubbin F. M. and Shearer C. K. (2013) A hydrogen-based oxidation mechanism  
889 relevant to planetary formation. *Earth Planet. Sci. Lett.* **380**, 88-97.
- 890 Shaw A. M., Hauri E.H., Behn M.D., Hilton D.R., Macpherson C.G. and Sinton J.M. (2012) Long-  
891 term preservation of slab signatures in the mantle inferred from hydrogen isotopes. *Nature*  
892 *Geosci.* **5**, 224-228.
- 893 Shearer C. K. and Floss C. (1999) Evolution of the Moon's mantle and crust as reflected in trace-  
894 element microbeam studies of lunar magmatism. In *Origin of the Earth and Moon* (R.  
895 Canup and K. Righter, eds.), Univ. of Arizona Press, Tucson, pp 339-359.
- 896 Shearer C. K. and Papike J. J. (2005) Early crustal building processes on the moon: Models for  
897 the petrogenesis of the magnesian suite. *Geochim. Cosmochim. Acta* **69**, 3445-3461.
- 898 Shearer, C. K., Elardo, S. M., Petro, N. E., Borg, L. E. and McCubbin, F. M. (2015) Origin of the  
899 lunar highlands Mg-suite plutonic rocks. An integrated petrology, geochemistry,  
900 chronology, and remote sensing perspective. *Amer. Mineral.*, **100**, 294–325.
- 901 Shervais J. W. and McGee J. J. (1999) KREEP cumulates in the western lunar highlands: Ion and  
902 electron microprobe study of alkali-suite anorthosites and norites from Apollo 12 and 14.  
903 *Amer. Mineral.* **84**, 806-820.
- 904 Snyder G. A., Taylor L. A. and Halliday A. N. (1995). Chronology and petrogenesis of the lunar  
905 highlands alkali suite: Cumulates from KREEP basalt crystallization. *Geochim. Cosmochim.*  
906 *Acta* **59**, 1185–1203.
- 907 Stéphan A. and Robert F. The negligible chondritic contribution in the lunar soils water. (2014)  
908 *Proc. Natl. Acad. Sci. USA* **111**, 15007-15012.

- 909 Stettler A., Eberhardt P., Geiss J., Grogler N. and Maurer P. (1973)  $Ar^{39}$ - $Ar^{40}$  ages and  $Ar^{37}$ - $Ar^{38}$   
910 exposure ages of lunar rocks. *Proc. 4<sup>th</sup> Lunar Sci. Conf.* 1865-1888.
- 911 Tartèse R. and Anand M. (2013) Late delivery of chondritic hydrogen into the lunar mantle:  
912 Insights from mare basalts. *Earth Planet. Sci. Lett.* **361**, 480-486.
- 913 Tartèse R., Anand M., Barnes J. J., Starkey N. A., Franchi I. A., and Sano Y. (2013) The  
914 abundance, distribution, and isotopic composition of Hydrogen in the Moon as revealed by  
915 basaltic lunar samples: Implications for the volatile inventory of the Moon. *Geochim.*  
916 *Cosmochim. Acta* **122**, 58-74.
- 917 Tartèse R., Anand M., McCubbin F.M., Elardo S.M., Shearer C.K., and Franchi J.A. (2014). Apatites  
918 in lunar KREEP basalts: The missing link to understanding the H isotope systematics of the  
919 Moon. *Geology* **42**, 363-366.
- 920 Taylor G.J., Warner R.D., Keil K., Ma M.-S., and Schmitt R.A. (1980) Silicate liquid immiscibility,  
921 evolved lunar rocks, and the formation of KREEP. *Proc. Conf. Lunar Highlands Crust*, 339-  
922 352.
- 923 Taylor G. J., Martel L. M. V, and Spudis P. D. (2012) The Hadley-Apennine KREEP Basalt Igneous  
924 Province. *Meteor. Planet. Sci.* **47**, 861-879.
- 925 Thompson A. B. (1992) Water in the Earth's upper mantle. *Nature* **358**, 295–302.
- 926 Turner G., Cadogan P. H., and Yonge C. J. (1973) Argon selenochronology. *Proc. 4<sup>th</sup> Lunar Sci.*  
927 *Conf.*, 1889-1914.
- 928 Tuttle O. F. and Bowen N. L. (1958) *Origin of granite in the light of experimental studies in the*  
929 *system NaAlSi<sub>3</sub>O<sub>8</sub>-KAlSi<sub>3</sub>O<sub>8</sub>-SiO<sub>2</sub>-H<sub>2</sub>O*, Geol. Soc. Am. Mem. **74**, 151 pp.
- 930 Ustunisik G., Nekvasil H., Lindsley D. H., and McCubbin F. M. (2015) Degassing pathways of Cl-,  
931 F-, H-, and S-bearing magmas near the lunar surface: Implications for the composition and  
932 Cl isotopic values of lunar apatite. *Amer. Min.* **100**, 1717-1727.
- 933 Wagner C., Deloule E. and Mokhtari A. (1996) Richterite-bearing peridotites and MARID-type  
934 inclusions in lavas from North Eastern Morocco: mineralogy and D/H isotopic studies. *Cont.*  
935 *Min. Petrol.* **124**, 406–421.
- 936 Warner R. D., Taylor G. J., Mansker W. L., and Keil K. (1978) Clast assemblages of possible deep-  
937 seated (77517) and immiscible-melt (77538) origins in Apollo 17 breccias. *Proc. 9<sup>th</sup> Lunar*  
938 *Planet. Sci. Conf.*, 941-958.
- 939 Warren P. H., and Wasson J. T. (1979) The origin of KREEP. *Rev. Geophys.* **17**, 73-88.
- 940 Warren P. H., Taylor G. J, Keil K., Shirley D. N. and Wasson J. T. (1983) Petrology and chemistry  
941 of two “large” granite clasts from the Moon. *Earth Planet. Sci. Lett.* **64**, 175-185.

- 942 Warren P. H., Jerde E. A. and Kallemeyn G. W. (1987) Pristine moon rocks: a “large” felsite and a  
943 metal-rich ferroan anorthosite. *Proc. 18<sup>th</sup> Lunar Planet. Sci. Conf.*, E303-E313.
- 944 Wieczorek M. A., Neumann G. A., Nimmo F., Kiefer W. S., Taylor G. J., Melosh H. J., Phillips R. J.,  
945 Solomon S. C., Andrews-Hanna J. C., Asmar S. W., Konopliv A. S., Lemoine F. G., Smith D. E.,  
946 Watkins M. M., Williams J. G. and Zuber M. T. (2013) The crust of the Moon as seen by  
947 GRAIL. *Science*, **339**, 671-675.
- 948 Yurimoto H., Kurosawa M. and Sueno S. A. (1989) Hydrogen analysis in quartz crystals and  
949 quartz glasses by secondary ion mass spectrometry. *Geochim. Cosmochim. Acta* **53**, 751-  
950 755.
- 951 Xia, Q-K., Deloule, E., Wu, Y-B., Chen, D-G. and Cheng, H. (2002) Anomalously high  $\delta D$  values in  
952 the mantle. *Geophys. Res. Lett.* **29**, 2008.
- 953
- 954
- 955
- 956
- 957
- 958
- 959
- 960
- 961
- 962
- 963
- 964
- 965
- 966

967 Table

Sample		ppm H <sub>2</sub> O	ppm H <sub>2</sub> O 2 $\sigma$	$\delta D$ ‰	$\delta D$ 2 $\sigma$	Corrected $\delta D$ ‰	$\delta D$ 2 $\sigma$	detect. limit (ppm H <sub>2</sub> O)	Instrument
14305, 656	apt1	23	1	799	650	735	652	13	NanoSIMS
	apt3 #2	136	4	491	320	481	320	13	NanoSIMS
	apt3 #3	41	1	-28	528	-65	528	13	NanoSIMS
	apt3 #4	37	1	973	513	934	514	13	NanoSIMS
	apt4	49	2	-76	458	-107	459	13	NanoSIMS
	apt5	54	2	-6	481	-34	481	13	NanoSIMS
	apt6	36	1	649	417	608	418	13	NanoSIMS
	apt7	53	2	-139	420	-168	420	13	NanoSIMS
14321, 1047	apt1 #1	<100		<i>n.d.</i>		<i>n.d.</i>		100	ims-1280
	apt1 #2	<100		<i>n.d.</i>		<i>n.d.</i>		100	ims-1280
	apt1 #3	82	2	247	415	231	415	24	NanoSIMS
	apt2 #1	<24		<i>n.d.</i>		<i>n.d.</i>		24	NanoSIMS
	apt2 #2	137	3	-108	364	-118	364	24	NanoSIMS
	apt4	93	2	-313	439	-327	439	24	NanoSIMS
	apt5	<24		<i>n.d.</i>		<i>n.d.</i>		24	NanoSIMS
	apt6 #1	66	2	943	356	925	356	24	NanoSIMS
	apt6 #2	76	2	806	317	790	317	24	NanoSIMS
14161, 7069	trapt #1	162	49	231	55	114	66	110	ims-1280
	trapt #2	189	57	265	56	165	62	110	ims-1280
14161, 7373	apt3	174	52	432	56	323	70	110	ims-1280
	apt2	<110		<i>n.d.</i>		<i>n.d.</i>		110	ims-1280
	apt1	<110		<i>n.d.</i>		<i>n.d.</i>		110	ims-1280
15403,71	apt1 #1	77	9	-589	78	-597	79	6	ims-1280
	apt1 #2	181	20	-721	48	-724	48	6	ims-1280
	apt1 #3	129	14	-749	56	-754	57	6	ims-1280
15404,51	apt6 #1	58	6	-428	135	-438	138	6	ims-1280
	apt6 #2	46	6	-640	80	-653	82	6	ims-1280
15404, 55	apt1 #1	134	4	-587	432	-592	432	13	NanoSIMS
	apt1 #2	267	9	-344	319	-346	319	13	NanoSIMS
	apt2 #1	76	2	-344	492	-352	492	13	NanoSIMS
	apt2 #2	99	3	-683	491	-689	491	13	NanoSIMS
	apt2 #3	99	3	-541	491	-547	491	13	NanoSIMS
	apt2 #4	69	2	-505	523	-514	523	13	NanoSIMS
15358,6	gls c4 #1	95	11	698	71	566*	88	10	ims-1280
	gls c4 #2	95	11	610	71	477*	86	10	ims-1280
	gls c1 #1	58	7	789	84	572*	124	10	ims-1280
	gls c1 #2	64	8	830	83	634*	117	10	ims-1280
76535, 52	apt1	75	7	791	66	639	93	22	ims-1280
76535,56	bigapt #1	62	6	572	79	388	106	22	ims-1280
	bigapt#2	86	8	475	110	342	103	22	ims-1280
	bigapt #3	<22		<i>n.d.</i>		<i>n.d.</i>		22	ims-1280
77538,16	apt1	175	55	335	74	304*	74	100	ims-1280
	apt2	188	55	411	74	383*	74	100	ims-1280

968 Table 1. Measured H<sub>2</sub>O abundances and  $\delta$ D values of lunar apatites and glasses\*. Multiple  
969 measurements on the same grain are indicated by a #. Italic font denotes measurements below  
970 our detection limit. *n.d.* - not detected. Analytical errors are  $2\sigma$ . Corrected  $\delta$ D values are those  
971 after correcting for the contribution of spallation-produced D, and uncertainty on the corrected  
972  $\delta$ D values is dominated by large uncertainty in the D production rate.

973 \*Exposure ages have not been determined for these samples. The CRE age estimates used  
974 here are described in section 3.2.

975

976

ACCEPTED MANUSCRIPT

977 **Figure Captions**

978 Fig. 1. Representative backscattered electron (BSE) images of samples described in this work.  
 979 Where visible, apatites are denoted by arrows. (a) Graphic intergrowth of quartz (dark gray)  
 980 and K-feldspar (light gray) in 14321, 1047. (b) Felsite-ferrobasalt silicate liquid immiscibility pair  
 981 in 77538, 16. The darker intergrowth is quartz and K-feldspar, while the bright areas are Fe-rich  
 982 olivine, pyroxene, and amorphous silica. Fe-Ni metal and ilmenite are also present. (c) Portion  
 983 of quartz monzogabbro 15404, 55. (d) Portion of quartz monzodiorite 14161, 7373. The  
 984 exsolved phase is inverted pigeonite, while the brightest phase is merrillite (Jolliff et al. 1999).  
 985 The bleb near the center of the image is intergrown silica and K-feldspar formed through  
 986 immiscibility. Bright squares are ion microprobe analysis pits. (e) Apatite-merrillite intergrowth  
 987 surrounded by plagioclase in troctolite 76535 56. The darkest phase is olivine. Round dark  
 988 marks in the apatite are pits from previous analyses. Note the large grain size. (f) Apatite-  
 989 merrillite intergrowth in an alkali anorthosite clast in breccia 14305, 656. The bright gray is  
 990 merrillite, the darker intergrowths are apatite (indicated by arrow). Darkest gray is plagioclase.

991  
 992 Fig. 2. Sample calibration curves for ims-1280 analysis. (a)  $^1\text{H}/^{18}\text{O}$  calibration curve for  $\text{H}_2\text{O}$  in  
 993 apatite and (b)  $^1\text{H}/^{30}\text{Si}$  calibration curve for  $\text{H}_2\text{O}$  in basaltic glass. Similar calibration curves were  
 994 used to calibrate NanoSIMS data.

995  
 996 Fig. 3. Apatite data for KREEP-rich intrusive samples, with  $2\sigma$  error bars. The spallation  
 997 correction can lower the  $\delta\text{D}$  of apatite by  $> 100\%$  in samples with long cosmic ray exposure  
 998 ages.

999  
 1000 Fig. 4. Plot showing  $\delta\text{D}$  value versus ppm  $\text{H}_2\text{O}$  content of apatite in this study (colored points)  
 1001 compared with literature apatite data (grayscale points, Greenwood et al. 2011; Tartèse et al.  
 1002 2013, 2014, Barnes et al. 2013, 2014a). Note the log scale on the x-axis.

1003

1004

1005 Fig. 5(a)(b) BSE images of KREEP basalt fragments containing quenched residual glass in  
1006 15358,6. Dark, straight-sided phase is plagioclase, medium gray is pyroxene, and the bright  
1007 areas are Fe-rich yellow glass. Silica (darkest gray) and ilmenite (white needles) are also  
1008 present. White squares indicate ion microprobe analysis pits. (c) Calculation of the increase in  
1009  $\delta D$  value due to hydrogen loss, constrained by the  $\delta D$  value measured in 15358 KREEP basalt  
1010 glass (corrected for crystallization). To reach the observed  $\delta D$  in 15358 requires loss of 85% of  
1011 an initial  $H_2O$  concentration of 115 ppm.

1012

1013 Fig. 6. Histogram of the lowest apatite  $\delta D$  measurement in lunar samples by rock type,  
1014 including literature data from Greenwood et al. (2011); Tartèse et al. (2013, 2014), and Barnes  
1015 et al. (2013, 2014a). The lowest  $\delta D$  apatite should represent the  $\delta D$  value least affected by  
1016 degassing, if degassing occurred. The range in  $\delta D$  value of Earth's mantle and CI and CM  
1017 chondrites is also shown (Boettcher et al., 1980; Michael 1998; Ahrens 1989; Deloule et al.,  
1018 1991; Bell and Rossman 1992; Thompson 1992; Graham et al., 1994; Jambon 1994; Wagner et  
1019 al., 1996; Xia et al., 2002; Alexander et al., 2012; Hallis et al., 2015). The protosolar  $\delta D$  value of  
1020  $\sim -865 \pm 32$  ‰ is from Geiss and Gloecker (1998). There appear to be at least three H reservoirs  
1021 in the lunar interior: an Earth-like reservoir, a moderately elevated reservoir, and a very low D  
1022 reservoir. The mare basalts would have had an initial undegassed  $\delta D$  signature compatible with  
1023 the Earth range,  $\sim 100$ ‰ (Tartèse and Anand 2013).

1024



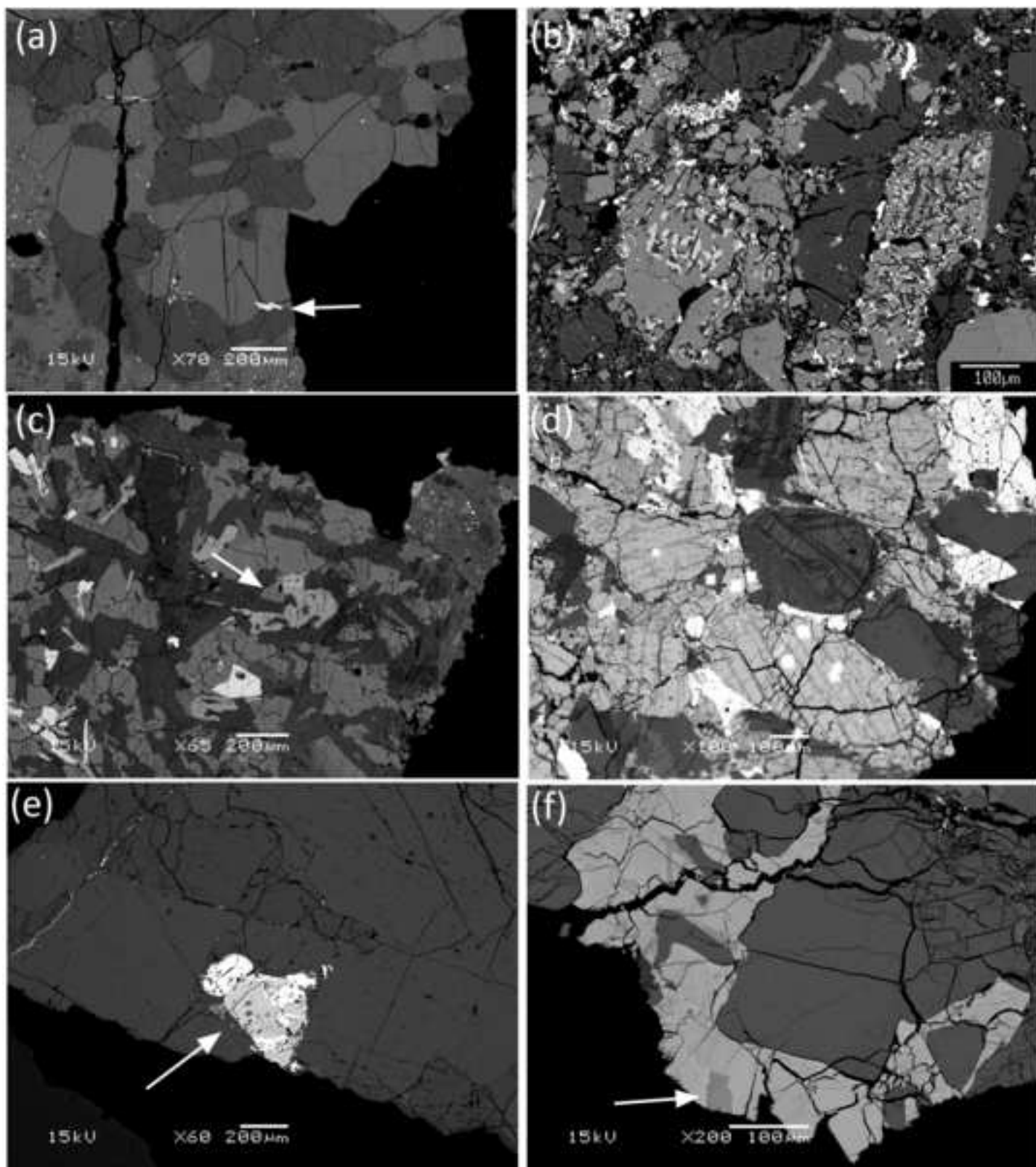
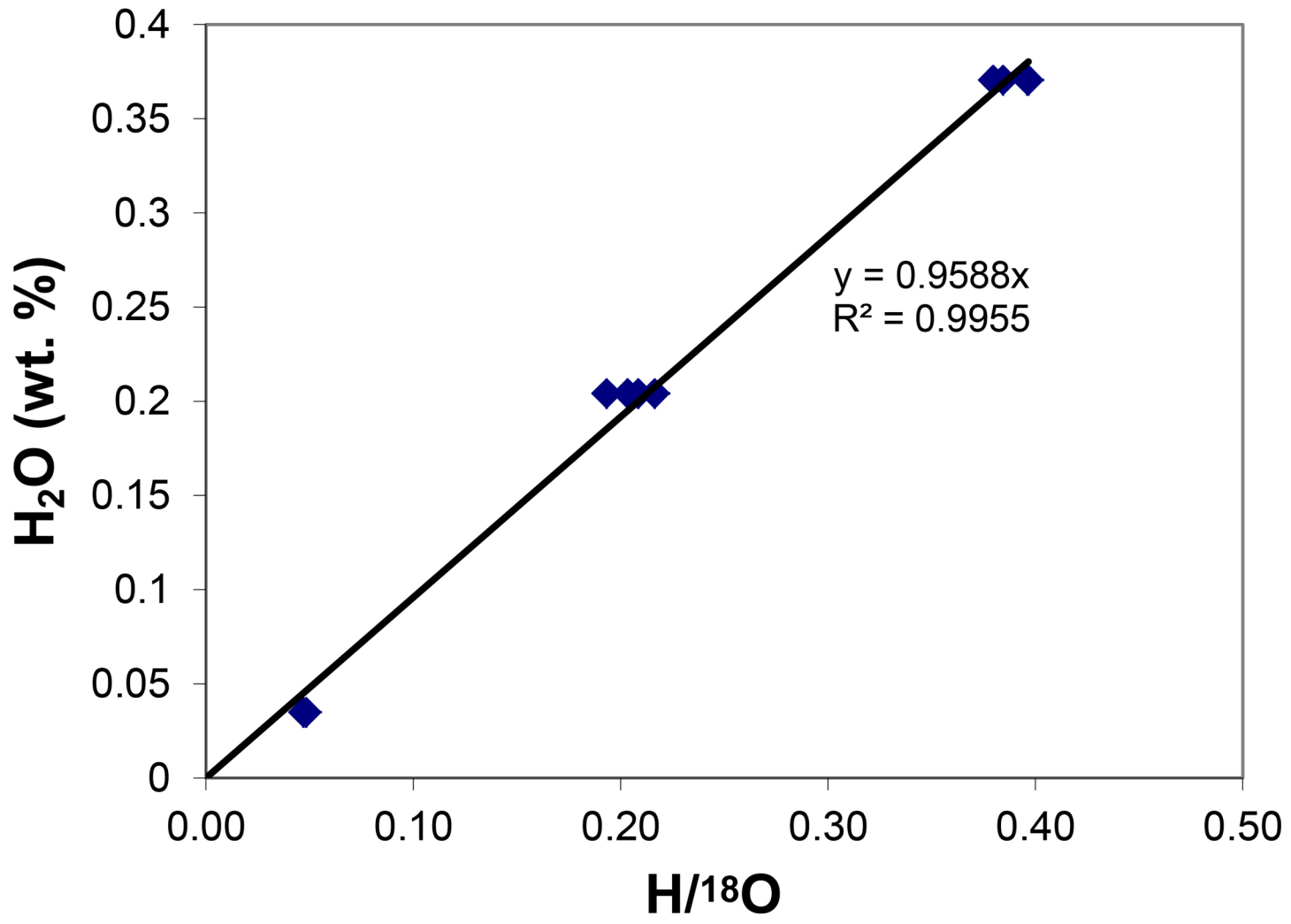


Figure 2

(a)

### H/<sup>18</sup>O calibration



(b)

### H/<sup>30</sup>Si calibration

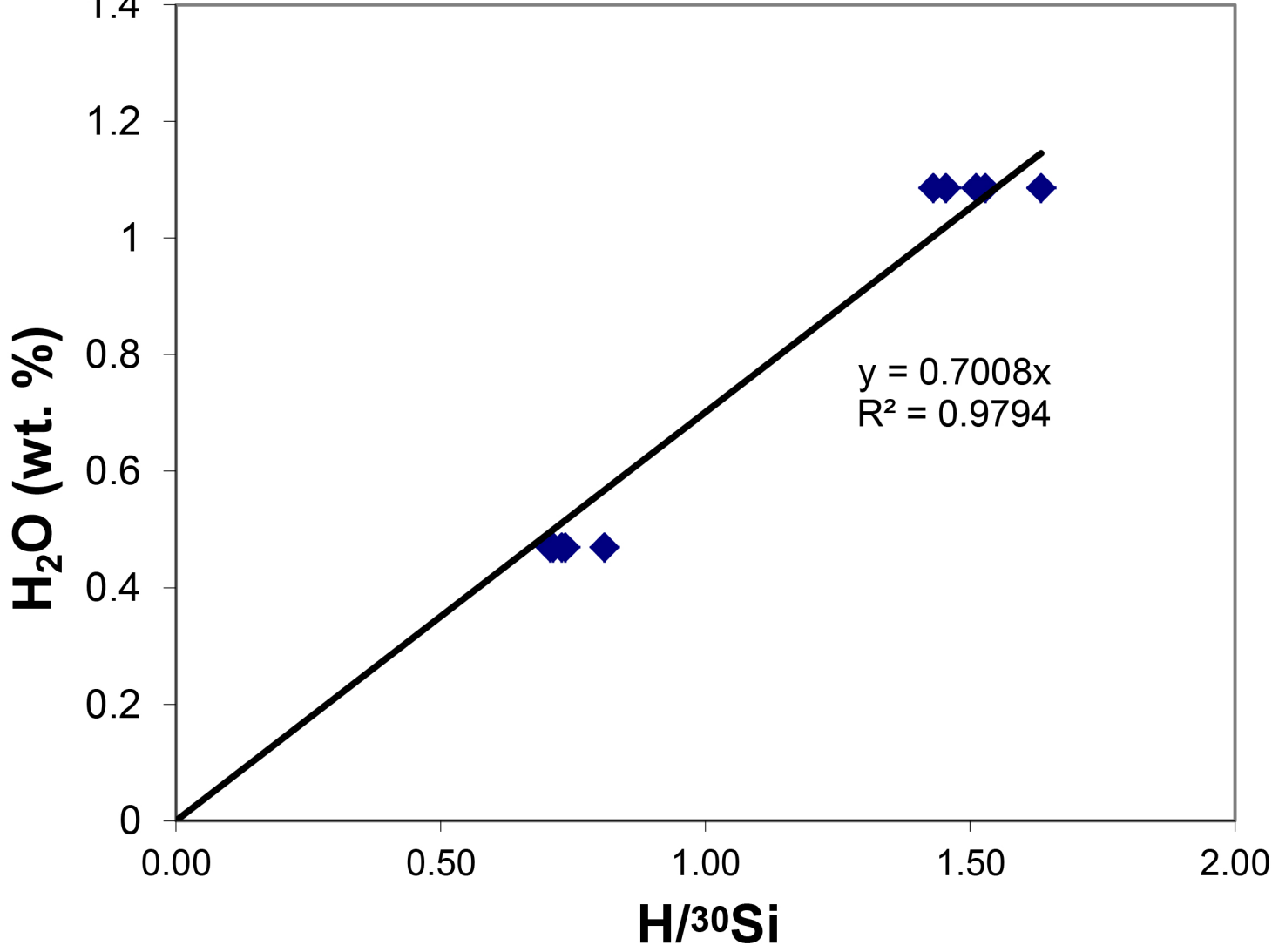


Figure 3

ACCEPTED MANUSCRIPT

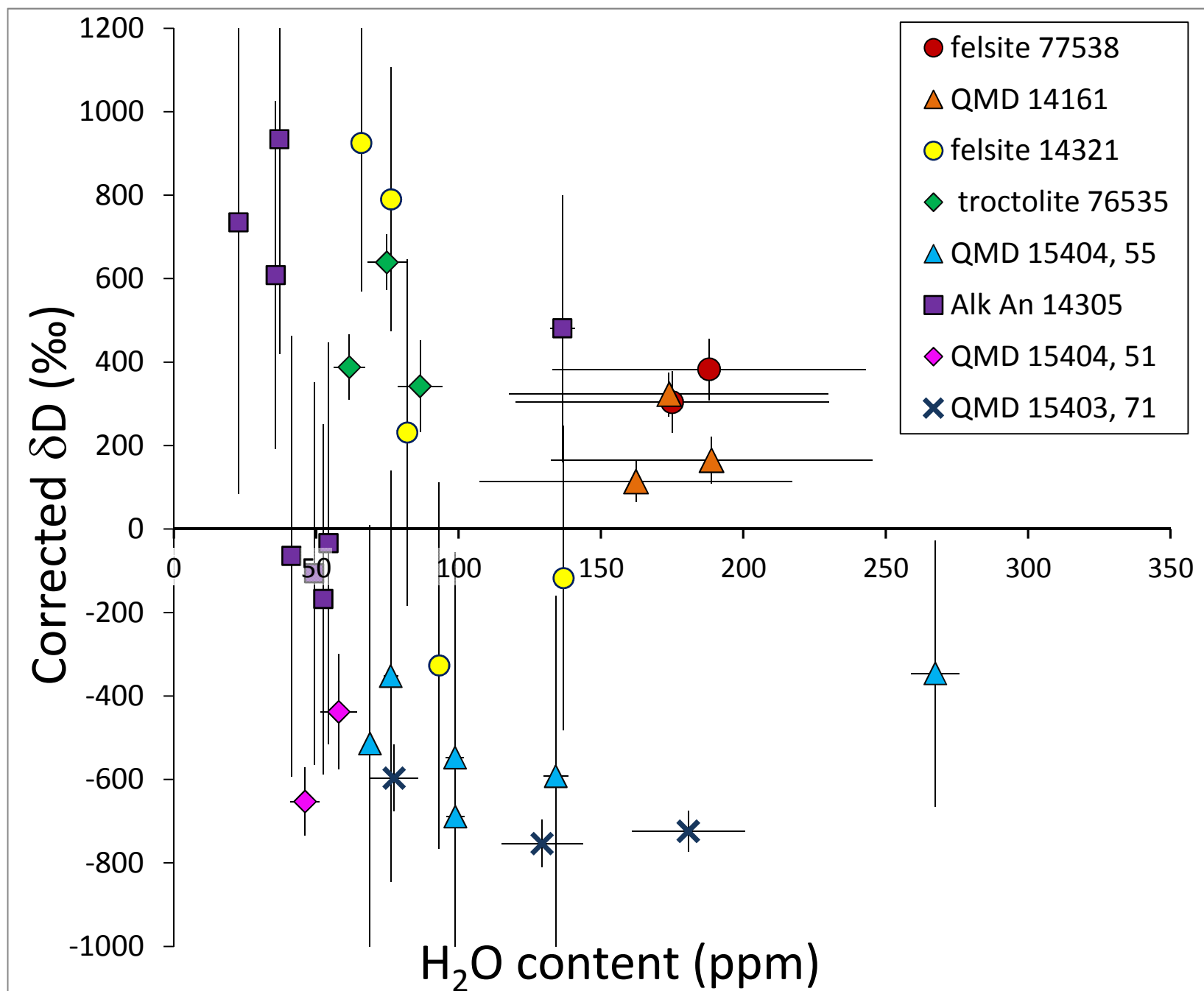


Figure 4

